Brain Struct Funct (2007) 212:269–301
DOI 10.1007/s00429-007-0158-9

ORIGINAL ARTICLE

Multimodal architectonic subdivision of the caudal ventrolateral prefrontal cortex of the macaque monkey

Marzio Gerbella · Abdelouahed Belmalih · Elena Borra · Stefano Rozzi · Giuseppe Luppino

Received: 12 March 2007 / Accepted: 28 August 2007 / Published online: 25 September 2007

Abstract The caudal part of the macaque ventrolateral prefrontal cortex (VLPF) is part of several functionally distinct domains. In the present study we combined a cyto- and a myeloarchitectonic approach with a chemoarchitectonic approach based on the distribution of SMI-32 and Calbindin immunoreactivity, to determine the number and extent of architectonically distinct areas occupying this region. Several architectonically distinct areas, completely or partially located in the caudal VLPF, were identified. Two areas are almost completely limited to the anterior bank of the inferior arcuate sulcus, a dorsal one—8/FEF—which extends also more dorsally and should represent the architectonic counterpart of the frontal eye field, and a ventral one—45B—which occupies the ventral half of the bank. Two other areas occupy the ventral prearcuate convexity cortex, a caudal one—area 8r—located just rostral to area 8/FEF and a rostral one—area 45A—which extends as far as the inferior frontal sulcus. Area 45A borders dorsally, in the proximity of the principal sulcus, with area 46 and, ventrally, with area 12. The present data show the existence of two distinct prearcuate convexity areas (8r and 45A), extending other architectonic subdivisions of the caudal VLPF and providing a new, multiarchitectonic frame of reference for this region. The present architectonic data, together with other functional and connectional data, suggest that areas 8/FEF, 45B and 8r are part of the oculomotor frontal cortex, while area 45A is a distinct entity of the VLPF domain involved in high-order processing of nonspatial information.

Keywords Architecture · Frontal lobe · Calbindin · SMI-32 · Myelin

M. Gerbella · A. Belmalih · E. Borra · S. Rozzi · G. Luppino (✉)
Dipartimento di Neuroscienze,
Sezione di Fisiologia, Università di Parma,
Via Volturno 39, 43100 Parma, Italy
e-mail: luppino@unipr.it

Introduction

The caudal part of the ventrolateral prefrontal cortex (VLPF) of the macaque brain, bordered dorsally by the principal sulcus (PS), caudally and ventrally by the inferior arcuate sulcus (IAS) and rostrally by the inferior frontal sulcus (IFS), is part of at least three functionally distinct domains. While its caudalmost part, the frontal eye field (FEF), is involved in oculomotor functions (Bruce and Goldberg 1984; Bruce et al. 1985), its dorsal part, close and within the PS, has been considered to play a role in visuospatial information processing (see, e.g., Levy and Goldman-Rakic 2000). Finally, the remaining rostral and ventral part is commonly included into a larger VLPF region involved in high-order processing of nonspatial information (Levy and Goldman-Rakic 2000; Passingham et al. 2000; Romanski 2004).

Architectonic studies of this region have resulted in markedly different parcellation schemes, in which both the number and the extent of the identified areas vary, raising conflicting interpretations on the architectonic definition of functionally different fields. For example, several investigators have quite consistently subdivided the prearcuate cortex into a dorsal and a ventral subdivision, designated by Walker (1940) as areas 8A and 45 (Fig. 1a), by Barbas and Pandya (1989) as dorsal and ventral area 8 (Fig. 1b) and by Preuss and Goldman-Rakic (1991) as areas 8A and 45 (Fig. 1c), respectively. However, Stanton et al. (1989)

have shown that the FEF, as functionally and cytoarchitectonically defined, occupies only a relatively small prearcuate sector, confined to the prearcuate bank and straddling over the caudalmost part only of both Walker's areas 8A and 45. Accordingly, Walker's area 45 (as well as ventral area 8 of Barbas and Pandya and area 45 of Preuss and Goldman-Rakic) is functionally and architectonically not homogeneous.

More recently, Petrides and Pandya (1994, 1999, 2002) have designated the caudalmost part of the prearcuate cortex as area 8, subdivided into a dorsal (8Ad) and a ventral (8Av) part (Fig. 1d). No distinction, however, was made between the prearcuate bank, where the FEF is located, and the adjacent convexity cortex. Furthermore, they designated as area 45 a cytoarchitectonic area, located ventral and rostral to area 8Av, characterized by the presence of large pyramidal cells in layer III. This area occupies the ventral part of the prearcuate bank, extending also rostrally and dorsally on the inferior frontal convexity. Accordingly, area 45, as defined by Petrides and Pandya, includes not only the ventral part of Walker's area 45, but also an inferior frontal convexity sector of controversial architectonic attribution, assigned by Walker (1940) to areas 46 and 12, by Preuss and Goldman-Rakic (1991) to area 12 and by Barbas and Pandya (1989) to areas 8 ventral and 46. Although considered as a unitary cytoarchitectonic entity, Petrides and Pandya designated as 45B the sector buried in the prearcuate bank and as 45A the sector located on the inferior frontal convexity.

On the basis of a comparative cytoarchitectonic analysis, Petrides and Pandya (1994, 2002; see also Petrides 2005) have proposed that area 45 is the putative homolog of the corresponding language area of the human brain. This proposal found support in connectional data (Petrides and Pandya 2002), showing that area 45, as a whole, is connected with auditory-related areas of the superior temporal gyrus (STG) and with multimodal areas of the upper bank of the superior temporal sulcus (superior polysensory area, STP). Recent electrophysiological data appear fully in line with this hypothesis, showing that in area 45 there are neurons with auditory responses to vocalization stimuli or integrating auditory and visual communicative information (Romanski et al. 2005; Sugihara et al. 2006).

Indirect evidence, however, suggests that area 45 is not homogeneous. Firstly, auditory-related areas of the STG (Petrides and Pandya 1988; Romanski et al. 1999a, b) and area STP (Seltzer and Pandya 1989) appear to project in the location of 45A, but not of 45B. Indeed,

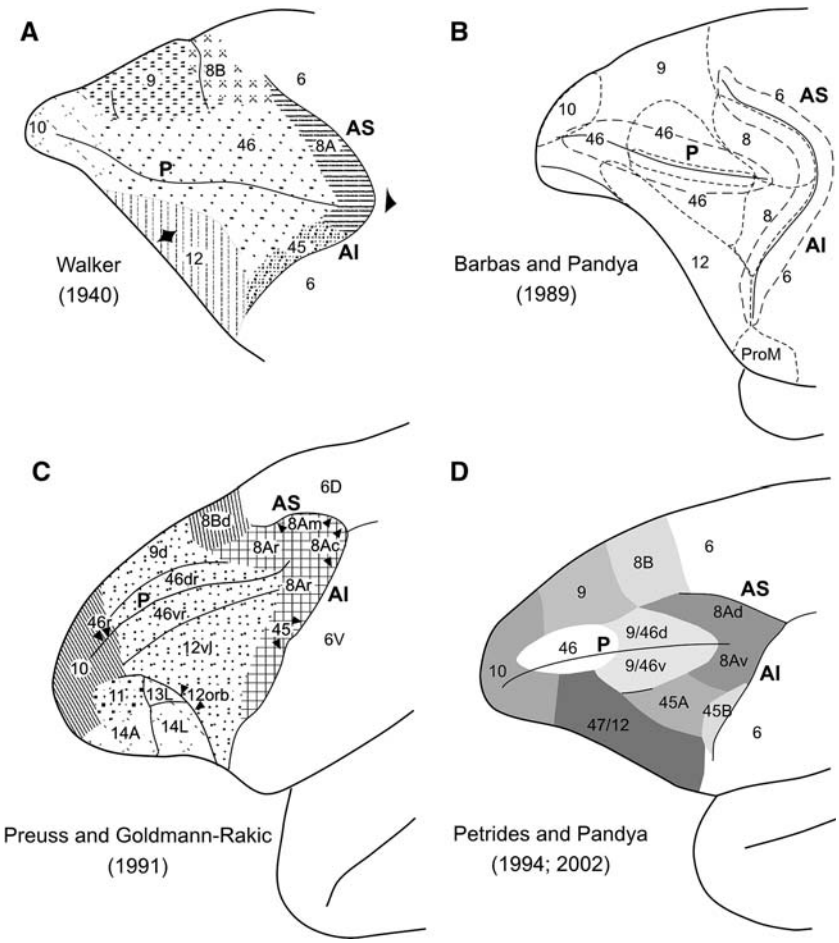

Fig. 1 Architectonic maps of the prefrontal cortex of the macaque monkey. The figure shows four different architectonic maps as proposed by: **a** Walker (1940); **b** Barbas and Pandya (1989); **c** Preuss and Goldman-Rakic (1991); **d** Petrides and Pandya (1994, 2002). *AI* inferior arcuate sulcus, *AS* superior arcuate sulcus, *P* principal sulcus

neurons responsive to communicative stimuli were recorded in the location of 45A, but not in 45B (Romanski et al. 2005; Sugihara et al. 2006). In contrast, tracer injections in the FEF (Huerta et al. 1987; Stanton et al. 1993), supplementary eye field (SEF) (Huerta and Kaas 1990; Luppino et al. 2003; Wang et al. 2005) or in motion sensitive visual areas of the caudal superior temporal sulcus (Maioli et al. 1998) produced labeling denser or almost exclusively located in the ventral prearcuate bank, in the location of 45B. Second, a recent functional magnetic resonance (fMRI) study in awake monkeys (Nelissen et al. 2005) has shown that observation of shapes or of actions made by others produced three anatomically segregated activation foci in the caudal VLPF, one observed in the location of 45B, another one in the location of 45A and the third close and within the PS. All together, these data suggest that: (a) 45B is functionally distinct from 45A; (b) 45A is a distinct entity and not part of areas 46, 12 or 8.

To resolve the question of whether the caudal VLPF comprises distinct cortical areas, possibly corresponding to the two sectors of area 45 of Petrides and Pandya (1994, 2002) and to the prearcuate convexity located rostral to the FEF, a thorough investigation of the neurophysiological and connectional features of this region is required. In order to analyze, report and correlate data from such experiments, a detailed preliminary analysis of the architectonic organization of the caudal VLPF is needed, so to obtain reliable structural maps which could subsequently be used as a frame of reference.

The present study was therefore undertaken in order to facilitate a more complete architectonic analysis of the caudal VLPF. To this end, we have combined the classical cyto- and myeloarchitectonic approaches with a chemoarchitectonic one, based on the distribution of SMI-32 and Calbindin immunoreactivity, which reveal different subpopulations of pyramidal and nonpyramidal cortical neurons (Campbell and Morrison 1989; Hendry et al. 1989). This last approach, by revealing regional differences in the organization of some aspects of the efferent and intrinsic components of the cortical circuitry, has been used in other studies as an architectonic tool to obtain additional support or independent evidence for the delineation of subdivisions in different cortical regions such as the prefrontal cortex (Carmichael and Price 1994; Dombrowski et al. 2001). Preliminary data have been presented in abstract form (Luppino et al. 2006).

Methods

Eighteen adult macaque monkeys (ten *Macaca nemestrina*, six *M. fascicularis* and two *M. mulatta*) of both sexes weighing between 5 and 8 kg were used in the present study. We did not observe any architectonic differences consistently related to either the species or the gender. In five monkeys (PR11, PR17, PR18, PR19 and PR20), brains were used only for the purposes of architectonic studies. M3 and M4 had been used as subjects in fMRI experiments (Nelissen et al. 2005). The remaining monkeys had been used in tract-tracing studies in which neural tracers were injected in different premotor or posterior parietal areas (see, e.g., Galletti et al. 2001; Luppino et al. 2001; Rozzi et al. 2006). Animal care and all experimental procedures were performed according to protocols approved by the Veterinarian Animal Care and Use Committee of the University of Parma and complied with the European law on the care and use of laboratory animals.

Histological procedures

Each animal was anesthetized with ketamine hydrochloride and subsequently received an i.v. lethal injection of sodium thiopental. Intracardial perfusion was initiated through the left cardiac ventricle with saline solution, followed by 3.5–4% paraformaldehyde. In all animals, but Cases PR18 and PR19, the perfusion was continued with 5% glycerol. All solutions were prepared in phosphate buffer 0.1 M, pH 7.4. The brain was then exposed, in case blocked on a stereotaxic apparatus, removed from the skull and photographed. All brains, but Cases PR18 and PR19, were placed in 10% (3 days) and then in 20% (3 days) buffered glycerol for cryoprotection. The right hemisphere of Case PR18 and the left hemisphere of Case PR19 were embedded in celloidin and cut at 50 μm tangentially to the IAS and parasagittally, respectively. All the other brains were cut frozen, at 60 μm, for a total number of 14 hemispheres coronally, 9 parasagittally, and 1 perpendicularly to the IAS. Table 1 summarizes the cases used for this study.

The tangential and the perpendicular to the IAS plane of sectioning were used in order to obtain optimal views of the architecture of the prearcuate bank, often poorly discriminated in the standard coronal plane, because of the oblique or almost vertical direction of the sulcus. In addition, sections cut tangential or perpendicular to the IAS offered optimal views of different rostro-caudal levels of the prearcuate bank and of the inferior frontal convexity, respectively, for the identification of boundaries between rostro-caudal subdivisions.

In all hemispheres, but Case M4, every fifth section was stained with the Nissl method (thionin, 0.1% in 0.1 M acetate buffer, pH 3.7). In Case M4, every third section of both hemispheres was processed for this staining. In nine animals (12 hemispheres, 7 of them cut coronally, 4 parasagitally, and 1 perpendicular to the IAS), sections

Table 1 Summary of cases studied

Case	Species	Hemisphere	Cut	Staining[a]
PR17	*Nemestrina*	Right	Perpendicular to IAS	Nissl, Myelin (120), SMI-32 (60), CB (60)
PR18	*Nemestrina*	Right	Tangential to IAS	Nissl (celloidin)
PR19	*Nemestrina*	Left	Parasagittal	Nissl (celloidin)
PR11	*Nemestrina*	Left	Parasagittal	Nissl, SMI-32 (60)
PR20	*Nemestrina*	Right	Parasagittal	Nissl, Myelin (120), SMI-32 (60), CB (60)
M4	*Mulatta*	Left	Parasagittal	Nissl, Myelin (60), SMI-32 (60)
		Right	Parasagittal	Nissl, Myelin (60), SMI-32 (60)
M3	*Mulatta*	Right	Parasagittal	Nissl, Myelin (120), SMI-32 (60), CB (60)
		Left	Coronal	Nissl, Myelin (120), SMI-32 (60), CB (60)
MEF16	*Fascicularis*	Right	Parasagittal	Nissl, SMI-32 (120), CB (60)
		Left	Parasagittal	Nissl, SMI-32 (120), CB (60)
MEF17	*Fascicularis*	Left	Parasagittal	Nissl, SMI-32 (60)
MEF18	*Fascicularis*	Left	Parasagittal	Nissl, SMI-32 (60)
Case 12	*Nemestrina*	Right	Coronal	Nissl, Myelin (120), SMI-32 (120), CB (60)
Case 18	*Nemestrina*	Right	Coronal	Nissl, Myelin (120), SMI-32 (60)
		Left	Coronal	Nissl, Myelin (60)
Case 13	*Fascicularis*	Right	Coronal	Nissl
		Left	Coronal	Nissl, SMI-32 (60)
Case 14	*Nemestrina*	Right	Coronal	Nissl
		Left	Coronal	Nissl
Case 20	*Nemestrina*	Right	Coronal	Nissl
		Left	Coronal	Nissl
Case 23	*Fascicularis*	Left	Coronal	Nissl, Myelin (60)
		Right	Coronal	Nissl
Case 29	*Fascicularis*	Left	Coronal	Nissl, Myelin (60)
Case 38	*Nemestrina*	Left	Coronal	Nissl, Myelin (60)

[a] Number in parentheses indicate the distance in micrometers from the Nissl-stained section

adjacent or close to those stained with thionin (see Table 1) were stained for myelin (Gallyas 1979).

The chemoarchitectonic study of the caudal VLPF was based on the analysis of the distribution of the immunoreactivity (ir) for the antibody SMI-32 and for the calcium-binding protein Calbindin (CB). SMI-32ir was analyzed in 11 animals (14 hemispheres, 4 of them cut coronally, 9 parasagitally, and 1 perpendicular to the IAS) and CBir in 5 animals (7 hemispheres, 2 of them cut coronally, 4 parasagittally, and 1 perpendicular to the IAS). In these hemispheres, every tenth section (Case 13l, SMI-32ir and Case 12, CBir) or every third section (Case M4) or every fifth section (all other hemispheres), adjacent or close to those stained with thionin (see Table 1) was immunoreacted as described in detail in previous studies (Geyer et al. 2000; Calzavara et al. 2005). Briefly, immediately after cutting, sections were rinsed in phosphate-buffered saline (PBS) for 10–15 min. Endogenous peroxidase activity was eliminated by incubation in a solution of 0.6% H_2O_2 and 80% methanol for 15 min at room temperature. Sections were rinsed in PBS for another 10–15 min and incubated in a solution of one of the following primary antibodies: mouse monoclonal SMI-32 (Sternberger Monoclonals, Baltimore, MA, USA) dilution 1:5,000 in 0.3% Triton (Sigma, St Louis, MO, USA), 2% normal horse serum (Vector, Burlingame, CA, USA), in PBS or monoclonal anti-calbindin D-28K (Swant, Bellinzona, Switzerland), dilution 1:5,000 in 0.3% Triton, 5% normal horse serum in PBS. After incubation and rinsing in PBS (15 min), sections were processed with the avidin–biotin method by using a Vectastain ABC kit (Vector) and 3,3′-diaminobenzidine (DAB, Sigma) as a chromogen. The reaction product was intensified with cobalt chloride and nickel ammonium sulphate. Immunoreacted sections were then mounted from saline, dehydrated in graded alcohols, and coverslipped. In order to avoid possible sources of

variability among sections from the same case, all sections selected for one type of immunostaining were processed all together in the same solutions.

Data analysis

Qualitative architectonic analysis

The cytoarchitectonic analysis was carried out with a Wild M420 Universal macroscope equipped with Apozoom objective for low-power observations, and with a Nikon Optiphot-2 and a Zeiss Axioscop 2 microscope for medium and high power observations. At least four researchers independently evaluated the material under study. The position of cytoarchitectonic borders between different areas, assigned by the different researchers, was in close agreement and only occasionally would differ by not more than 500 μm. In each section, the outer and inner cortical borders (pial and white matter borders) and the location of the boundaries between the various identified cytoarchitectonic areas were plotted with the aid of a software developed in our laboratory. By using inductive displacement transducers, mounted on the *X* and *Y* axes of the microscope stage, the Cartesian coordinates of points located along the outer and inner cortical borders and in correspondence with cytoarchitectonic boundaries were acquired and digitalized separately through a computer board. These coordinates were then graphically visualized all together as section outlines, gray–white matter borders and cytoarchitectonic borders. The qualitative analysis of myelin-stained and SMI-32 and CB immunoreacted sections was carried out independently from the cytoarchitectonic analysis, by using the same procedures. Myelo- and immuno-architectonic borders were then correlated with cytoarchitectonic borders, by using a camera lucida attached to the microscope. The boundaries between cortical layers, traced from Nissl-stained sections were transferred to the immunostained sections by using a camera lucida attached to the microscope.

Quantitative analysis of SMI-32 and CB immunoreactivity

The distribution of SMI-32ir in the caudal VLPF was analyzed quantitatively in three hemispheres (PR17, C18r, and MEF16l), from three monkeys of two different macaque species and cut in three different planes of section. This analysis was aimed to evaluate the density of immunopositive cells in different cytoarchitectonic areas and cortical layers. By using the above mentioned computer based charting system, immunopositive neurons were plotted, at a magnification of 200×, in cortical transverses 250 μm wide from the pial surface through the entire cortical thickness. In each hemisphere, eight transverses were plotted for each of five different caudal VLPF areas, as cytoarchitectonically defined. Thus, this analysis was based on a total number of 40 transverses from each hemisphere and a total number of 24 transverses (8 transverses per case) for each area. The plotted transverses were selected from different sections and different parts of each area. By using a camera lucida attached to the microscope, borders between different cortical layers were transferred on the plots from adjacent Nissl-stained sections.

For each area, the density of the SMI-32 immunopositive cells was analyzed separately for layers II/III and V, where virtually all these neurons were observed. Density was defined in terms of number of immunopositive cells, plotted in a given layer, divided by the thickness of that layer expressed in millimeters, for a transverse 250 μm wide. Although in the supragranular layers SMI-32 immunopositive cells were all located in layer III, layer II and III were considered together because of the difficulty in setting the border between them. The obtained data were tested with a two-way ANOVA for repeated measures (factors: Area, Layer, 5×2 ANOVA), followed by post hoc Bonferroni correction for multiple comparisons.

The distribution of CBir in the caudal VLPF was analyzed quantitatively in three hemispheres (PR17, M3l, and MEF16l), from three different macaque species and cut in three different planes of section, in terms of density of immunopositive cells in different cytoarchitectonic areas and cortical layers. As reported in other studies (for review, see Hof et al. 1999), CB immunopositive neurons included two main populations of cells. One, by far the most represented, consisted of darkly and more lightly stained nonpyramidal cells, the other of pyramidal cells, most of them only lightly stained. All CB immunopositive nonpyramidal and pyramidal cells were plotted separately, at a magnification of 400×, in cortical transverses 250 μm wide from the pial surface through the entire cortical thickness. The total number of transverses analyzed and the criteria for their selection were the same as in the analysis of SMI-32ir described above.

Two types of analyses were carried out in order to compare the distribution of CB immunopositive cells across different areas. The first analysis aimed to evaluate the density of the two different subpopulations of CB immunopositive cells (nonpyramidal and pyramidal neurons) in the studied areas. To this purpose, the total number of each of these two types of cells, plotted in transverses 250 μm wide, was divided by the cortical thickness expressed in millimeters. According to the plane of sectioning, the border of layer VI with the white matter was sometimes difficult to draw with precision, because of an oblique cut of the cortex (e.g., the prearcuate bank in coronal sections).

Thus, we considered for this and the following analysis the cortical thickness from the pial surface to the border between layers V and VI. In this respect, it should be noted that in all areas under study, layer VI CB immunopositive neurons were very sparse and homogenously distributed. The obtained data were tested with a two-way ANOVA for repeated measures (factors: Cell type, Area, 2×5 ANOVA) followed by post hoc *t* test with Bonferroni correction for multiple comparisons. The second analysis aimed to obtain an estimate of the differences in the laminar distribution of CB immunopositive nonpyramidal neurons in each area. To this purpose, the number of these cells, plotted in a given layer of a cortical transverse 250 μm wide, was divided by the thickness of that layer expressed in millimeters. Given that the distribution of CB immunopositive nonpyramidal cells in supragranular layers was highly heterogeneous, with a much higher concentration in layer II and the uppermost part of layer III, layers II and III, considered as a whole, were subdivided into four sublaminae of equal thickness. Thus, six different layers/sublayers were analyzed: the four layer II/III sublaminae, layer IV and layer V. The obtained data were tested with a two-way ANOVA for repeated measures (factors: Area, Layer/Sublamina, 5×6 ANOVA), followed by post hoc Bonferroni correction for multiple comparisons. The distribution of CB immunopositive pyramidal neurons was not analyzed in terms of laminar distribution. These cells were mostly located in the lower half of layer III and their laminar distribution was similar across different areas.

Architectonic maps

In all cases used in the present study, architectonic maps of the caudal VLPF were obtained by reporting the location of architectonic borders on drawings of dorso-lateral views of the studied hemispheres.

Furthermore, in order to obtain more realistic views of the location and extent of the identified architectonic areas, data from individual sections, spaced 600 μm, obtained with the above-mentioned computer based charting system, were imported into a 3D reconstruction software (Bettio et al. 2001). By using this software, the individual sections were firstly manually translated or rotated for their alignment. The alignment was based on the location of the track left in the white matter by a needle inserted orthogonally to the plane of sectioning and of several cortical and subcortical anatomical landmarks. Furthermore, local non-linear transformations were applied to correct distortions due to the histological processing. Finally, a 3D rendering of the cortical surface was created showing the extent of the identified architectonic areas. The obtained 3D reconstructions could be also re-sliced in any desired plane, for comparing data from hemispheres cut with different planes of sectioning, or dissected to expose cortical surfaces buried within sulci. The location of areas lying on the VLPF cortical convexity was visualized in standard dorso-lateral views of the hemispheres. Areas located in the prearcuate bank were visualized in non-standard views of the hemispheres in which the bank was exposed with appropriate dissection of the 3D reconstruction.

Finally, to have an estimate of the interindividual variability and the average location of the identified architectonic areas with respect to the IAS, the PS and IFS, an average architectonic map of the caudal VLPF was created as follows. Firstly, in the drawings of dorso-lateral views of 20 hemispheres from 7 *M. nemestrina* and 3 *M. fascicularis* we measured the total length of the IAS and of the superior arcuate sulcus (SAS). For each hemisphere, the SAS and the IAS were divided in ten segments of equal length. The coordinates of the end points of each of these segments, the tip of the PS and the end points of the IFS were introduced in a Cartesian space with the zero centered on the genu of the arcuate sulcus (GAS) and the *X* axis running over the tip of the PS. A template hemisphere was then created, based on the averages of the coordinates of each of these points, measured in all the considered hemispheres (Fig. 2a). The IFS was included in the template, although present only in 70% of the hemispheres analyzed. Finally, architectonic maps obtained from ten representative hemispheres cut coronally (seven *M. nemestrina* and two *M. fascicularis*), were warped in order to fit with the template hemisphere. To this purpose, we used a Matlab script to apply a deformation to each of the ten reconstructions, based on a linear interpolation of a triangle mesh formed by the four corners of the image and other reference points defined by the user, using the Matlab "griddata" function (Watson 1992). This method is based on a Delaunay triangulation of the data. In each case and in the template hemisphere three groups of reference points were set for the warping procedure, in addition to the four corners of the images and the GAS (Fig. 2b). The first group included the tip of the SAS and two other points, located at 1/3 and 2/3 of the sulcus. The second group included the tip of the IAS and two other points, located at 1/3 and 2/3 of the sulcus. The third group included the tip of the PS and two other points, located at 1/3 and 2/3 of the distance between the tip of the PS and the GAS. In this way, composite architectonic maps were generated, providing information on the reliability of the architectonic maps, obtained in ten different hemispheres, and on the interindividual variability of the location and extent of the identified architectonic areas, with respect to the major anatomical landmarks of the caudal VLPF.

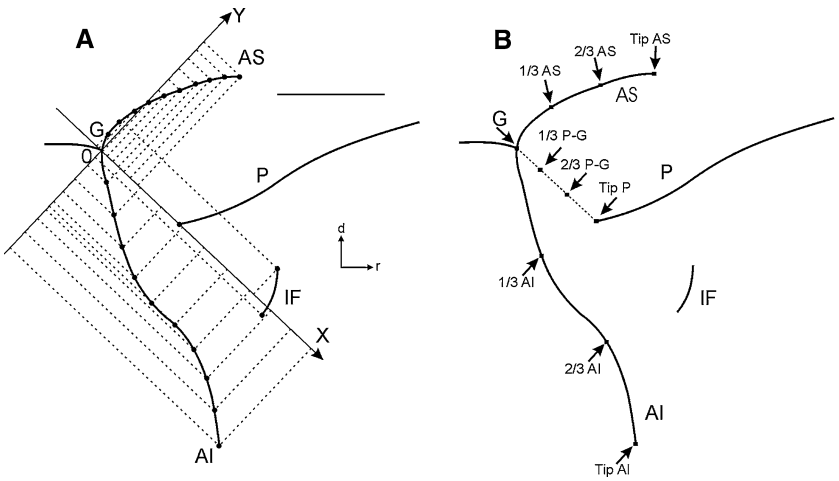

Fig. 2 Construction of a template caudal VLPF and warping procedure for the generation of average architectonic maps. **a** drawing of the arcuate, principal and inferior frontal sulcus of the template caudal VLPF, represented in a Cartesian space centred on the genu of the arcuate sulcus, with the *X* axis connecting the genu with the tip of the principal sulcus. *Dots* represent the reference points used to generate the template. The *X*–*Y* coordinates of each dot were obtained by averaging the *X*–*Y* coordinates of the corresponding points of 20 different hemispheres. **b** Drawing of the template caudal VLPF showing the reference points used for warping each hemisphere onto the template hemisphere. The reference points are indicated by *squares* located at the four corners of the image, on the genu of the arcuate sulcus and at different locations along the arcuate sulcus and the line connecting the genu with the tip of the principal sulcus (*dashed line*), as described in the methods. *d* dorsal, *G* genu of the arcuate sulcus, *IF* inferior frontal sulcus, *r* rostral. Other abbreviations as in Fig. 1. *Scale bar* = 5 mm in **a** (applies also to **b**)

Photographic presentation

Photomicrographs shown in the present study were obtained by capturing images directly from the sections with a digital camera attached to the macroscope or to the microscope. Individual images were then imported in Adobe Photoshop, in which they were assembled into digital montages and reduced to the final enlargement. Image brightness and contrast were adjusted, if necessary, to reproduce the original histological data.

Results

Several architectonically distinct areas were identified, totally or partially located in the VLPF region delimited caudally by the fundus of the IAS, rostrally by the IFS, dorsally by the ventral crest of the PS and ventrally by the reflection of the dorso-lateral convexity onto the orbital surface.

Two of these areas are almost completely limited to the anterior bank of the IAS, at different dorso-ventral levels. One more dorsal area partially extends also in the superior prearcuate bank and should represent the architectonic counterpart of the FEF. This area has been referred to as area 8/FEF. One more ventral area occupies the ventral half of the anterior bank of the IAS and has been referred to as area 45B. Two other areas lie on the ventral prearcuate convexity cortex. One is located just rostral to area 8/FEF on the caudalmost part of the prearcuate convexity cortex and has been referred to as rostral area 8 (8r). The other, located rostral to area 8r and dorsal to area 45B, extends in the caudal VLPF as far as the IFS. This area has been referred to as area 45A. Area 45A borders dorsally, in the proximity of the PS with area 46 and, ventrally, in the proximity of the orbifrontal cortex, with area 12.

The identification of these areas has been primarily based on the analysis of Nissl-stained material. In this respect, it should be noted the following (see also Gregoriou et al. 2006). First, very often architectonic features change gradually from one region to another, usually in the range of about 0.5 mm. Accordingly, borders between areas, shown as arrows in the photomicrographs, indicate the intermediate points of these transitions. Second, some general and primary architectonic features, e.g., cell density and size, often show some interindividual variability. Accordingly, in the present study the definition of the cytoarchitectonic areas was mostly based on *relative* changes in single layer characteristics and in individual histological elements, observed within individual cases, which could be reliably and consistently observed across different cases. By employing this approach and by using different planes of sectioning, we were able to set reliable cytoarchitectonic criteria, despite the interindividual variability of cytoarchitectonic features.

To seek a possible additional and independent validation of the presently proposed subdivision of the caudal VLPF, the cytoarchitectonic approach has been combined with the

myeloarchitectonic and two different and complementary chemoarchitectonic approaches. This multiarchitectonic analysis has been very helpful in providing independent and complementary criteria for the characterization of the various identified caudal VLPF areas.

The analysis of myelin-stained material, in spite of some variability in the quality of fiber staining from one section to another, showed that, in general, the various cytoarchitectonic areas differed also in their myeloarchitectonic features. These differences, mostly based on the presence and staining intensity of the inner and outer horizontal fiber plexi ("bands of Baillarger"), provided further support to the cytoarchitectonic subdivision of the caudal VLPF. Changes in myeloarchitectonic features, however, were rather more gradual with respect to changes the cytoarchitectonic features. Thus, this approach was less effective than the cytoarchitectonic one, for a precise delineation of architectonic borders.

SMI-32 is an antibody which reveals in the primate neocortex subpopulations of layers III and V pyramidal cell bodies and proximal portions of their apical and basal dendrites (Campbell and Morrison 1989). SMI-32ir displays specific regional and laminar distribution patterns and is an effective architectonic tool in the macaque for the delineation of occipito-parietal (e.g., Hof and Morrison 1995), temporal (Cusick et al. 1995), agranular frontal (e.g., Geyer et al. 2000), cingulate (Nimchinsky et al. 1996) and prefrontal (Carmichael and Price 1994) areas. We found SMI-32ir very helpful for a precise delineation and further characterization of the different caudal VLPF areas. In this respect, it should be noted that, likely because of slight differences in the fixation and immunostaining procedures, some variability was observed, from one case to another, in the absolute staining intensity of the immunopositive cells and neuropil. Nevertheless, qualitative analysis based on relative changes, within individual cases, in the number of immunopositive cells and laminar position and intensity of cell and neuropil immunostaining, showed that the various caudal VLPF cytoarchitectonic areas very well corresponded to different chemoarchitectonic fields. These observations were supported by quantitative analysis of the density of immunopositive pyramids in layers II/III and V.

CBir is present in a subpopulation of cortical nonpyramidal and pyramidal neurons (e.g., DeFelipe et al. 1989; Hendry et al. 1989). Other studies have shown that CBir displays regional differences in the distribution of immunopositive nonpyramidal or pyramidal cells and can be used for the characterization of different sensory (Kondo et al. 1999), temporal (Kondo et al. 1994, 1999) and prefrontal (Carmichael and Price 1994; Condé et al. 1994; Dombrowski et al. 2001) areas. In agreement with these studies, we found that also in the caudal VLPF immunopositive nonpyramidal neurons were by far more represented than the immunopositive pyramidal ones. In general, all over the caudal VLPF, immunopositive nonpyramidal neurons were highly concentrated in layer II and in the uppermost part of layer III, less concentrated in the remaining part of layer III and relatively sparse in layers IV–VI. These neurons showed a high variability in staining intensity, from very dense to very light, and the proportion of densely stained cells appeared to be related to the overall staining intensity of the immunoreacted material. In contrast, immunopositive pyramidal cells were virtually all weakly stained and mostly distributed in layer III. Qualitative and quantitative analysis of the CB immunoreacted material showed that, in spite of a similar general pattern of CBir distribution, differences in the number and laminar distribution of CB immunopositive cells can be very helpful for the characterization of different caudal VLPF regions and areas.

In the next sections, the architectonics of each caudal VLPF area will be firstly described in terms of cyto- and myeloarchitectonic features and distribution of SMI-32ir. The distribution of CBir in the various caudal VLPF areas will be described comparatively in a separate section.

Fig. 3 Cytoarchitecture of the caudal VLPF. **a–e** Low-power photomicrographs of a series of Nissl-stained coronal sections, in a caudal to rostral order, taken from Case 18r. **a1–e1** Low-power photomicrographs of a series of Nissl-stained coronal sections, taken from Case 12r at AP level similar to those shown in **a–e**. In all photomicrographs, *arrows* indicate the borders between cytoarchitectonic areas. *Scale bar* = 1 mm in **a** (applies to all photomicrographs). Section orientation in **a1**, applies to all photomicrographs and section drawings. The levels at which the sections were taken are indicated by *dashed lines* on the drawings of the dorsolateral views of the hemispheres. *Dashed boxes* on the section drawings indicate the locations of the photomicrographs. *Dashed boxes* in **b–d** indicate the location of the higher magnification views of Fig. 15. *Dashed boxes* in **b**1 and **d**1 indicate the location of the higher magnification views of Fig. 8. *C* central sulcus, *Cg* cingulate sulcus, *IP* intraparietal sulcus, *l* lateral, *LF* lateral fissure, *LO* lateral orbital sulcus, *Lu* lunate sulcus, *MO* medial orbital sulcus, *ST* superior temporal sulcus. Other abbreviations as in Figs. 1 and 2

Area 8/FEF

Area 8/FEF was identified in the caudalmost part of the prearcuate cortex. In coronal sections (Fig. 3a, a1), this cortical sector is cut almost tangentially to the cortical surface, so that its architecture was poorly delineated. Nevertheless, it was evident, even at a very low power view, that this sector hosts a cytoarchitectonic area characterized by the presence of numerous, relatively large layer V pyramids. Parasagittal, perpendicular to the IAS and tangential to the arcuate sulcus sections (Figs. 4, 5, 6, 7), provided optimal and complementary views of the architectonics of this sector. The combined analysis of these three types of sections showed that the presence of

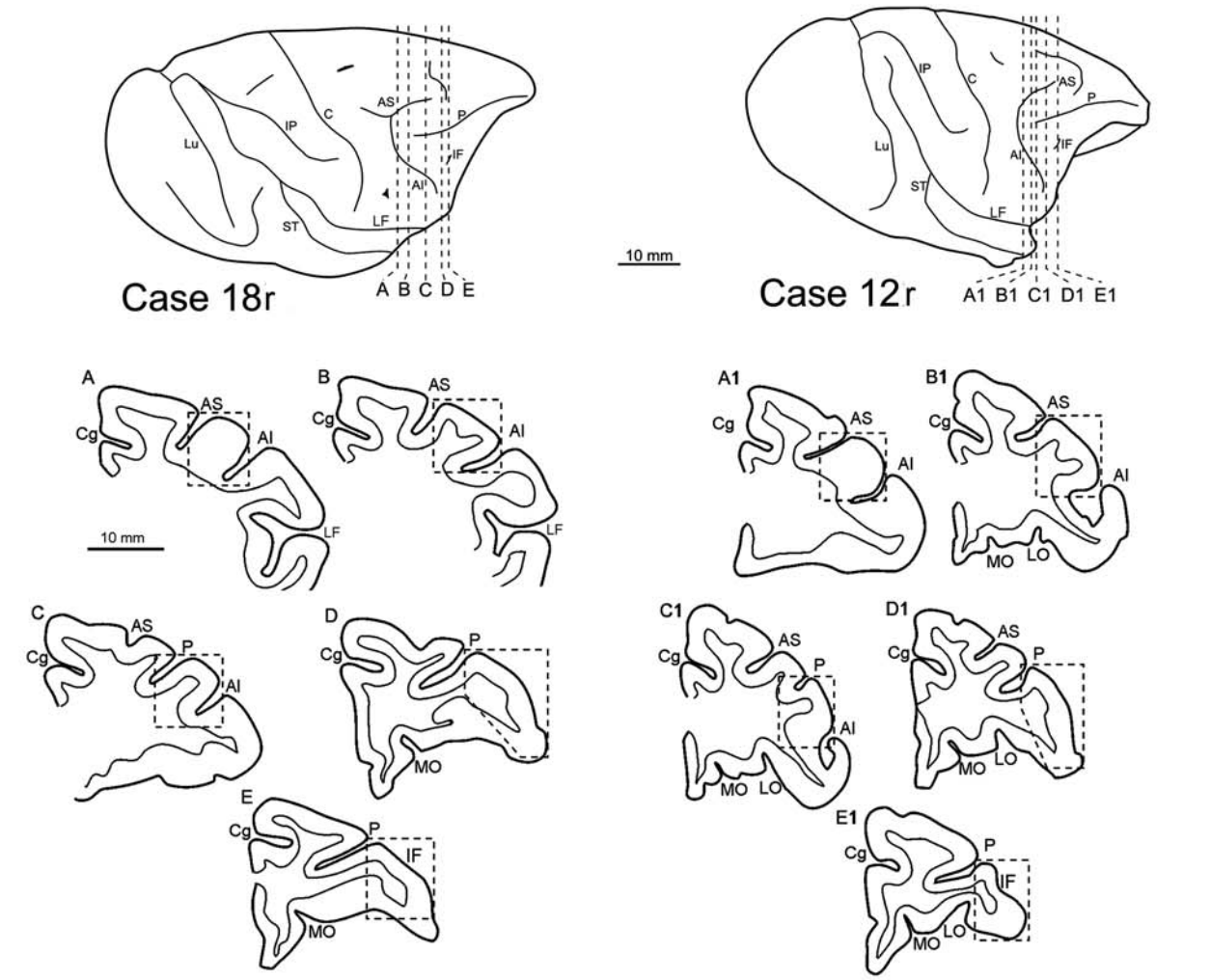
Case 18r
Lu
IP
C
AS
P
IF
AI
ST
LF
A B C D E
Case 12r
10 mm
A1 B1 C1 D1 E1
A
B
C
D
E
A1
B1
C1
D1
E1
Cg
AS
AI
P
IF
LF
MO
LO
10 mm

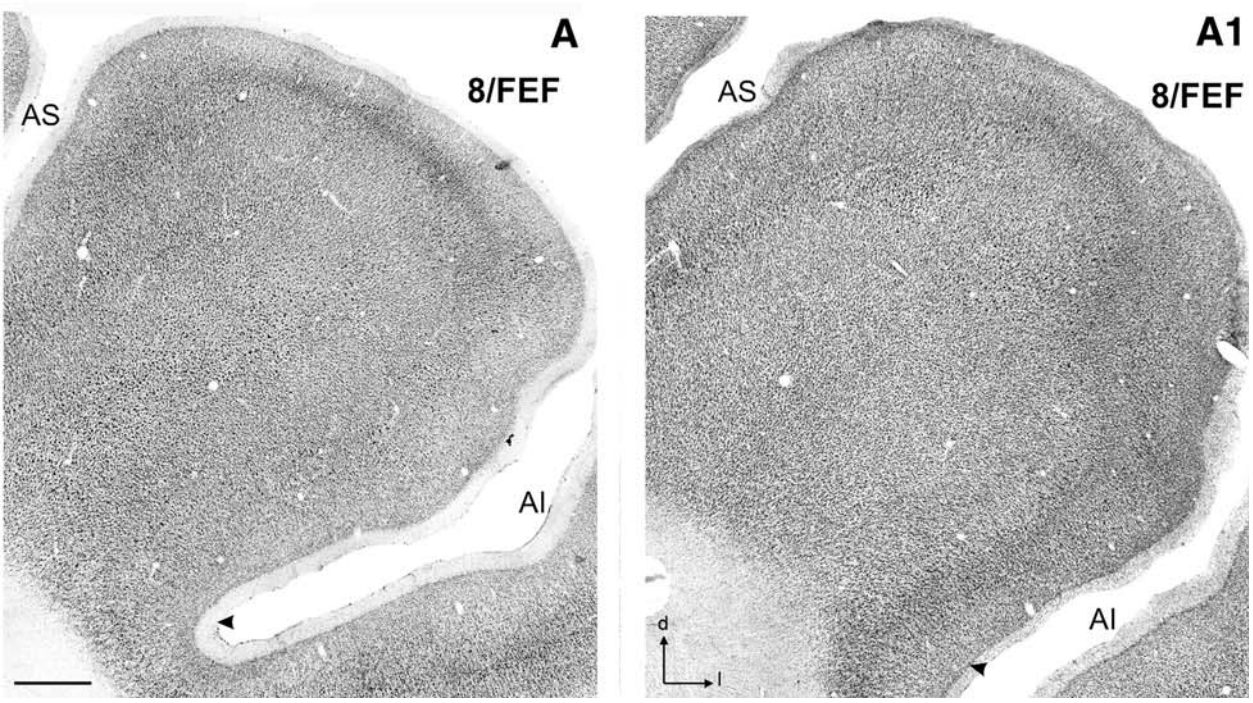
A
8/FEF
AS
AI
A1
8/FEF
AS
AI
d
l

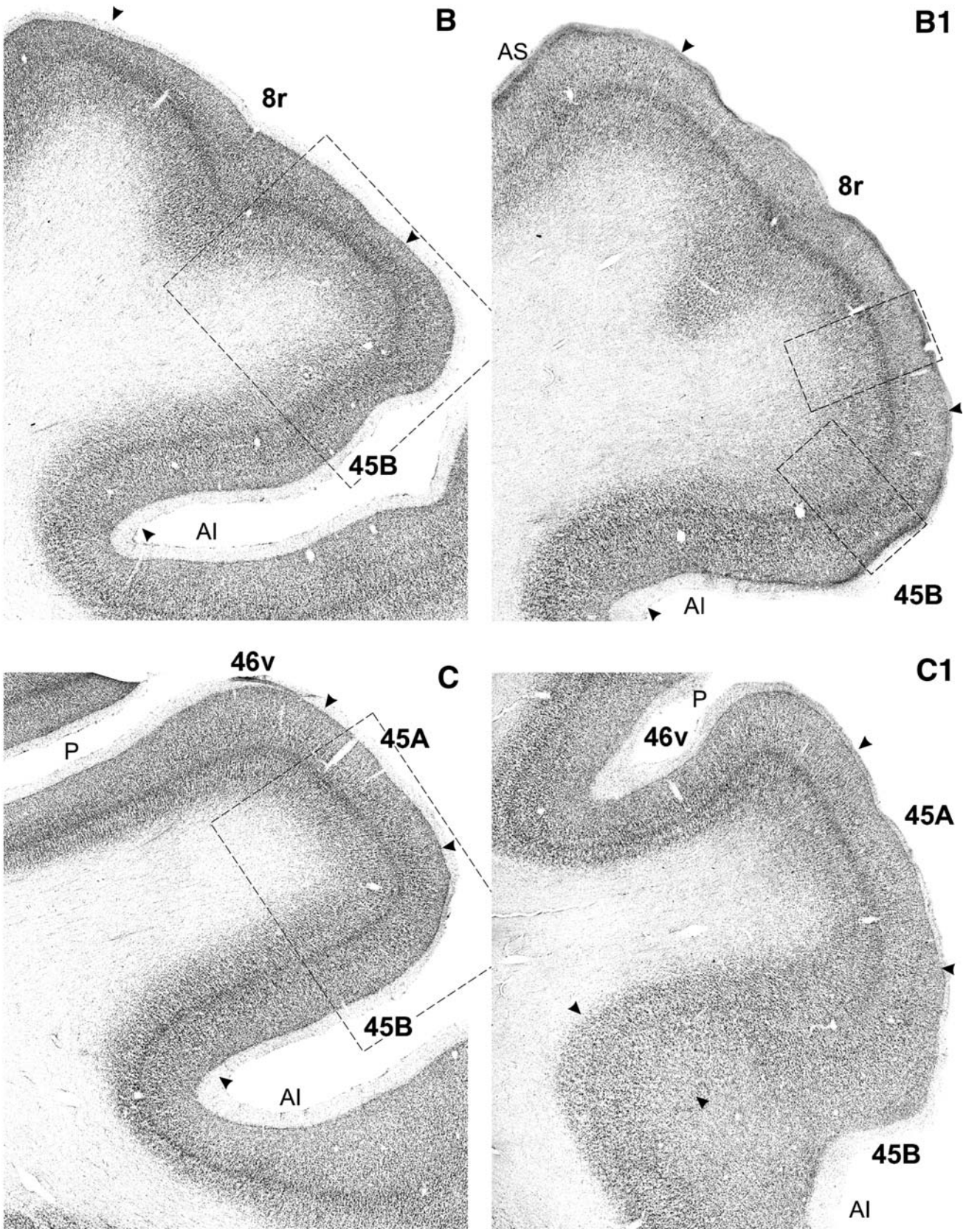

Fig. 3 continued

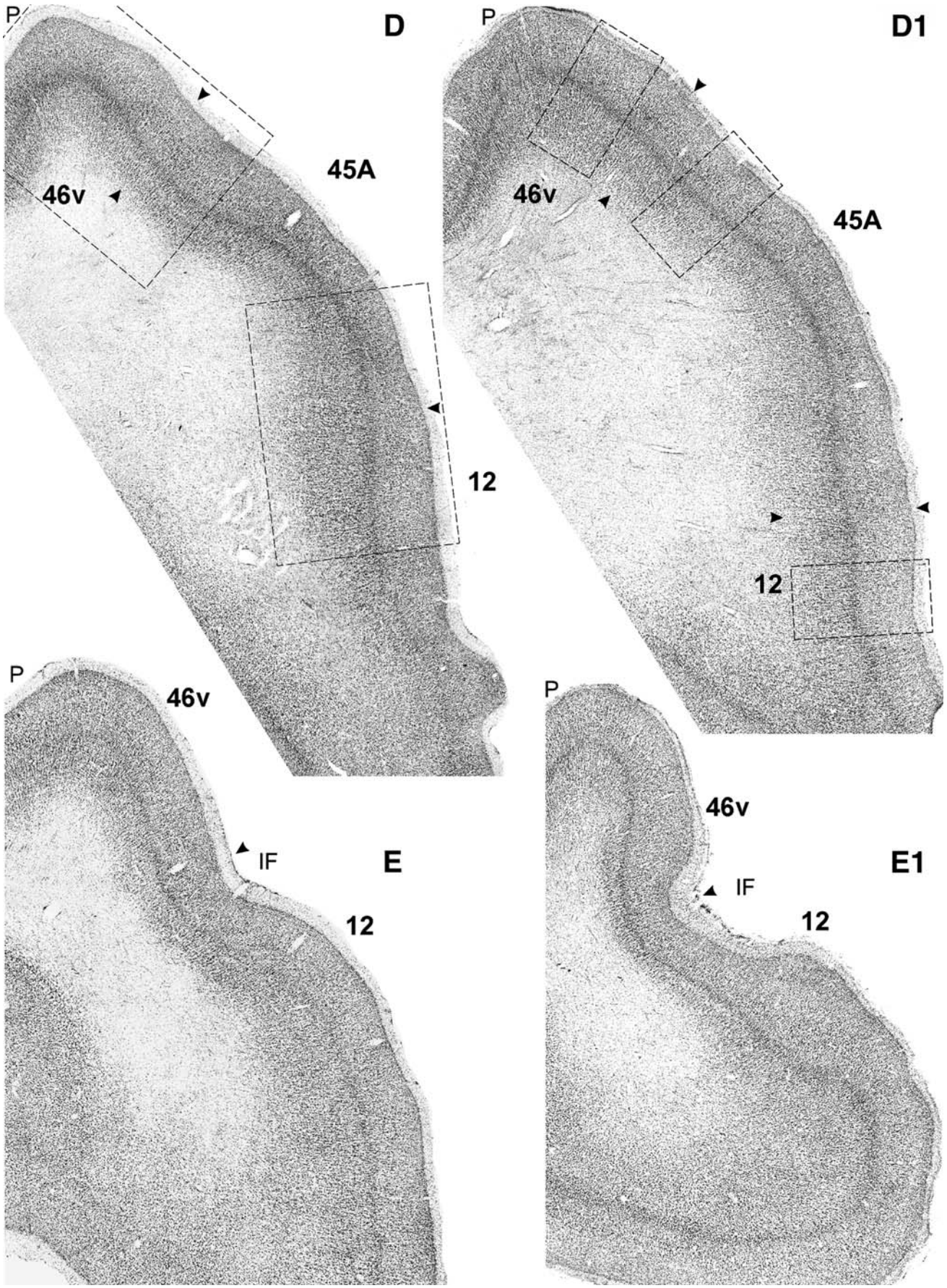

Fig. 3 continued

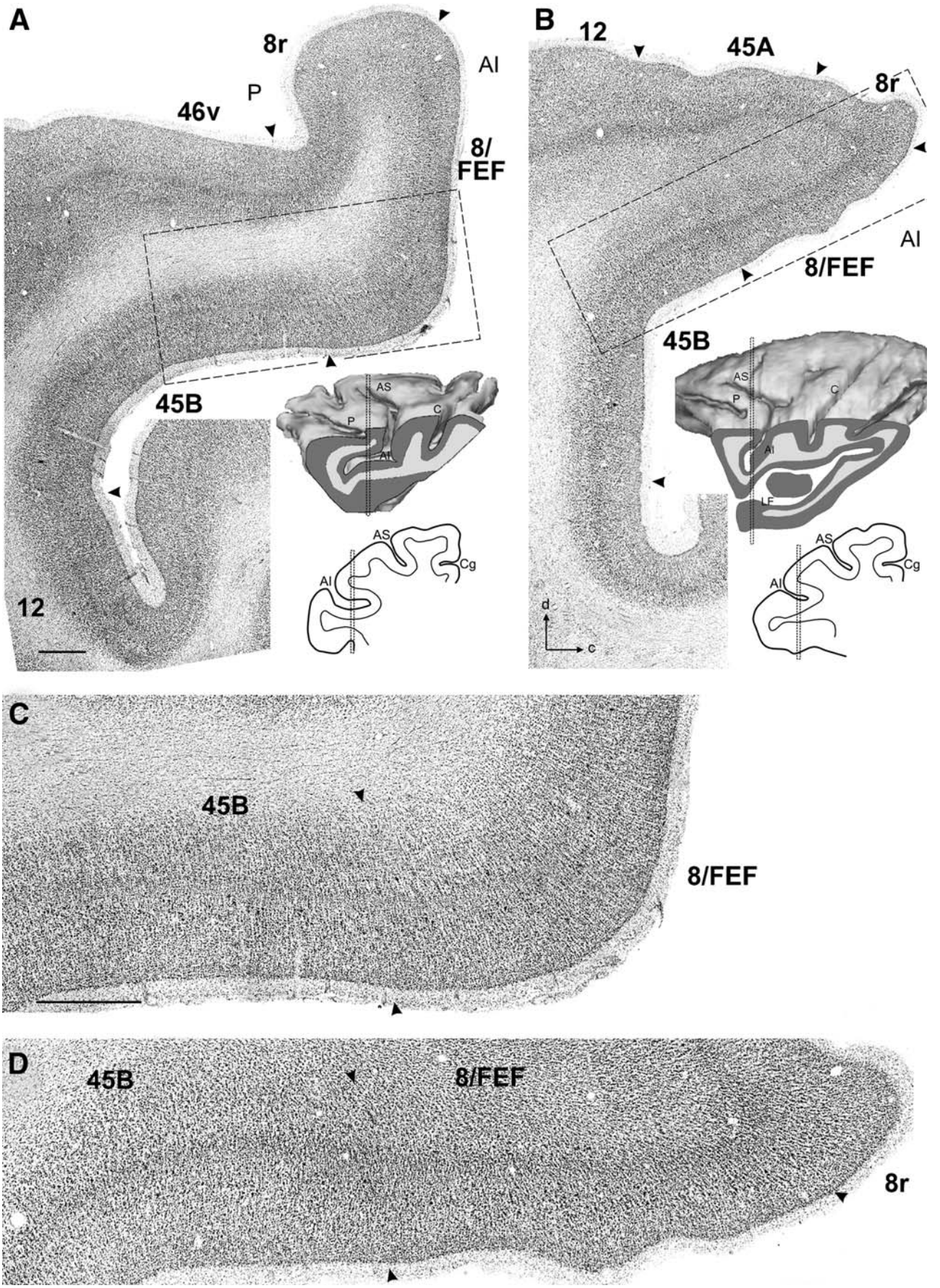
A
8r
Al
P
46v
8/
FEF
45B
12
AS
P
C
Al
AS
Cg
Al
B
12
45A
8r
Al
8/FEF
45B
AS
P
C
Al
LF
AS
Cg
Al
d
c
C
45B
8/FEF
D
45B
8/FEF
8r

◀ **Fig. 4** Cytoarchitecture of the caudal VLPF. **a** Low-power photomicrographs of a Nissl-stained parasagittal section taken from Case M4l. **b** Low-power photomicrograph of a Nissl-stained parasagittal section taken from PR20, shown as from a *left hemisphere*. *Scale bar* = 1 mm in **a** (applies also to **b**). Section orientation in **b**, applies also to **a**. In both **a** and **b**, a 3D reconstruction of the hemisphere shows the level at which the section was taken and a drawing of a coronal section, re-sliced from the 3D reconstruction, shows the AP level of the border between areas 8/FEF and 45B. The *thin dashed box* on the 3D reconstruction indicates the level of the re-sliced coronal section. The *thin dashed box* on the section drawing indicates the mediolateral level of the photographed parasagittal section. **c** Higher magnification view of the cytoarchitectonic transitions between areas 8/FEF and 45B, taken from the sections shown in A. **d** Higher magnification view of the cytoarchitectonic transitions between areas 8/FEF and 45B, taken from the sections shown in **b**. The location of the photomicrographs in **c** and **d** is indicated by *dashed boxes* in **a** and **b**, respectively. *Scale bar* = 1 mm in **c** (applies also to **d**). *c* caudal; other abbreviations and conventions as in Figs. 1 and 3

large layer V pyramids is a unifying and identifying architectonic feature of a cytoarchitectonic area almost completely buried in the caudalmost part of both the dorsal and the ventral prearcuate bank. Though varying in absolute size across different cases (see, e.g., Figs. 4c, d, 6a, 7b), within each individual case these large layer V pyramids were: (a) usually larger than those in layer III; (b) the largest layer V pyramids observed anywhere in the caudal VLPF; (c) comparable in size with the large layer V pyramids observed in the caudally adjacent rostral premotor cortex. Additional architectonic features of area 8/FEF (Fig. 8a) were a barely discernible layer II and a layer III displaying relatively larger pyramids in its lower part, larger and more numerous in the ventral part of this area. Layer IV was evident, but relatively thin. Comparison of parasagittal and tangential sections with similar sections presented by Stanton et al. (1989) showed that the architectonic features and the location of this area were very well coincident with those of the FEF as cytoarchitectonically and functionally defined.

The analysis of myelin-stained sections (Fig. 9a), showed that area 8/FEF was the heaviest myelinated area seen anywhere in the caudal VLPF. In particular, this area (Fig. 10a, a1) was characterized by very close and conspicuous vertical bundles of fibers, extending up to the superficial cortical layers and a dense and course plexus of mixed vertical and horizontal fibers, which represented an identifying myeloarchitectonic feature of this area.

Area 8/FEF could be very clearly delineated with SMI-32ir. Low-power photomicrographs from coronal, parasagittal and perpendicular to the IAS (Figs. 11, 12, 13) sections and higher magnification views in Figs. 12c, e, 13d, and 14a, show the presence, in layer III, of dense, darkly stained immunopositive pyramids of different size and dense. Immunopositive apical dendrites were darkly stained and mostly confined to the lower half of this layer. Layer V displayed a band of immunopositive neuropil and many, relatively large, darkly immunostained pyramids. Although comparisons with Nissl-stained sections suggested that, within each individual case, these immunopositive pyramids do not represent the entire population of large layer V pyramids, area 8/FEF was, in any case, the only caudal VLPF area displaying a consistent population of large, darkly stained, layer V immunopositive cell bodies. The observation of a relatively richness in immunopositive layer V pyramids in this area was confirmed by the quantitative analysis. The two-way ANOVA performed on the values of laminar density of SMI-32 immunopositive cells showed a significant main effect of Area [$F(4;68) = 29.438$, $p < 0.001$] and Layer [$F(1;17) = 23.242$, $p < 0.001$] and a significant interaction effect (Area × Layer) [$F(4;68) = 17.474$, $p < 0.001$]. Post hoc analysis showed that the density of layer V immunopositive pyramids in area 8/FEF was significantly higher ($p < 0.001$) than that of all the studied areas, but area 8r (Fig. 14g).

Area 45B

Area 45B was identified in the ventral prearcuate bank, rostro-ventrally to area 8/FEF, only slightly extending on the convexity cortex (Fig. 3b, b1, c, c1). The major identifying cytoarchitectonic feature of this area was the presence of large and deeply stained pyramids in the lower part of layer III, evident even at very low power view. Higher magnification views (Figs. 4c, d, 6b, c, 8b) show that these cells were relatively sparse, clearly standing out against an overall population of layer III pyramids relatively homogeneous in cell size and density. Most of them were located in the lowest part of layer III, in the proximity of the border with layer IV. Although varying in number and size across different individuals, within each case these outstanding pyramids were always larger than those in layer V and of a size at least comparable, if not larger, than that of the large layer V pyramids observed in area 8/FEF. Area 45B was also characterized by a thin, but definable layer II and a well developed, cell dense layer IV (Fig. 8b). Layer V was cell sparse, not clearly sublaminated and virtually all populated by small pyramids, with only occasional larger cells in its lower part.

The border between areas 8/FEF and 45B run roughly in the coronal plane at about 1–2 mm caudal to the tip of the PS. Accordingly, it was better defined in parasagittal, perpendicular and tangential to the arcuate sulcus sections, where the appearance of very large pyramids in layer IIIc and the virtual disappearance of large layer V pyramids represented reliable criteria for the definition of the transition from area 8/FEF to area 45B (Figs. 4c, d, 6b, 7b).

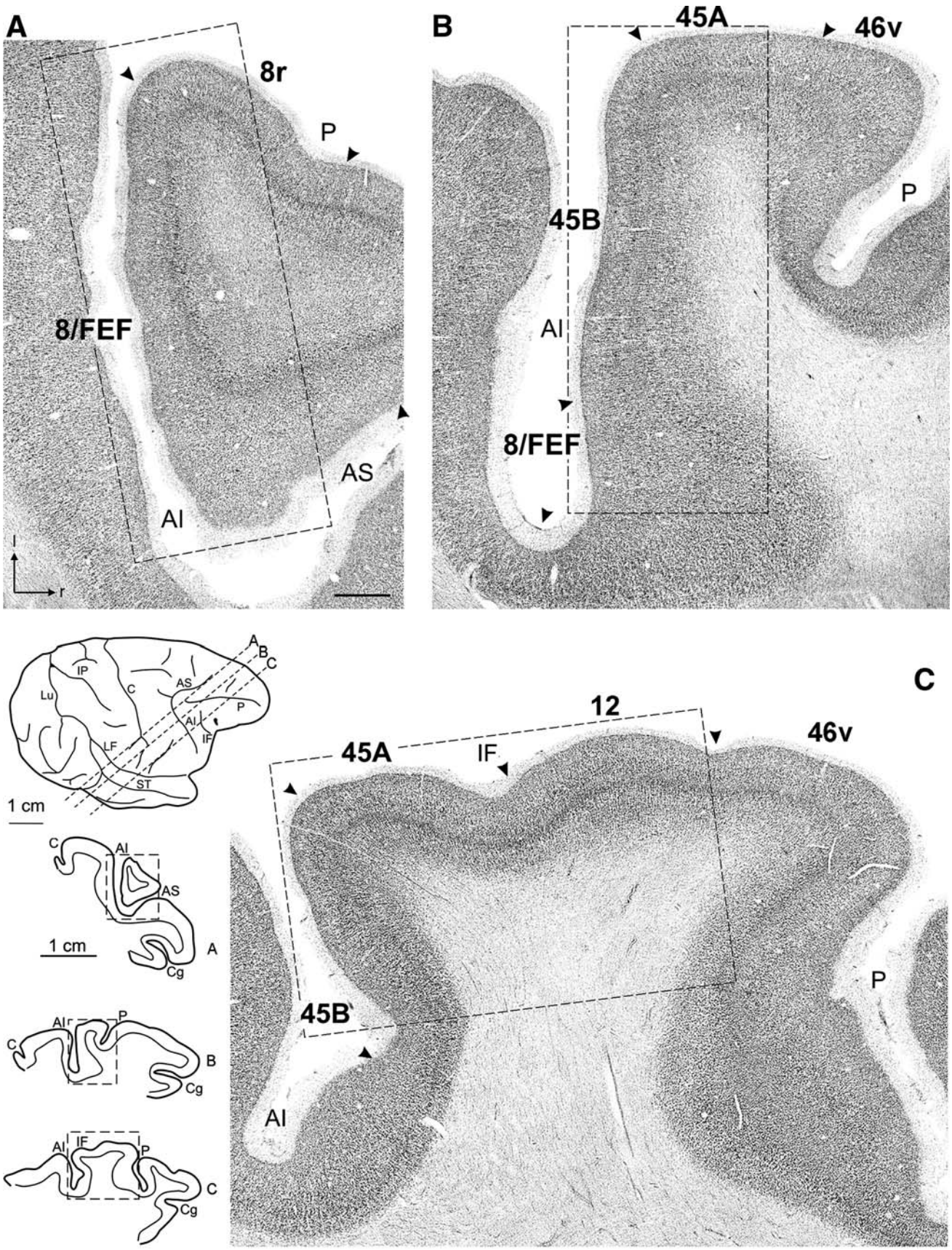
A
8r
P
8/FEF
AS
AI
l
r
B
45A
46v
P
45B
AI
8/FEF
A
B
C
IP
Lu
C
AS
P
AI
IF
LF
ST
1 cm
C
AI
AS
1 cm
A
Cg
AI
r
P
C
B
Cg
AI
IF
P
C
Cg
C
12
45A
IF
46v
P
45B
AI

◀ **Fig. 5** Cytoarchitecture of the caudal VLPF. **a–c** Low-power photomicrographs of three Nissl-stained perpendicular to the IAS sections, in a dorsal to a ventral order, taken from Case PR17. *Scale bar* = 1 mm in **a** (applies to **a–c**). Section orientation in **a**, applies to **a–c**. The levels at which the sections were taken are indicated by *dashed lines* on the drawing of the dorso-lateral view of the hemisphere. *Dashed boxes* on the section drawings indicate the locations of the photomicrographs. *Dashed boxes* on the photomicrographs indicate the location of the higher magnification views of Fig. 6. Other abbreviations and conventions as in Figs. 1, 2, and 3

The analysis of tangential sections showed that this border very well coincided with the rostral border of the FEF, defined by Stanton et al. (1989). Area 45B occupied virtually the entire extent of the prearcuate bank ventral to area 8/FEF (Fig. 4a, b, 7a). For most of its extent, it bordered ventrally, in close correspondence with the fundus of the IAS, with an agranular or dysgranular cortical area, which extended caudally in the ventral premotor cortex (Fig. 3b, c). In correspondence with the ventralmost part of the IAS, area 45B bordered ventrally with a granular area which, in most cases, occupied the very rostralmost part of the ventral postarcuate cortex, slightly invading the prearcuate bank (Figs. 4a, 7a, c). This granular area was considered to be part of area 12 and may correspond to area 12l, as defined by Carmichael and Price (1994).

Myeloarchitectonic analysis showed that area 45B (Fig. 9b, c) was relatively heavily myelinated, though less than area 8/FEF. In particular, this area displayed dense vertical bundles of fibers, thinner than in area 8/FEF, tending to stop at the level of a very dense and clearly delimited outer band of Baillarger (Fig. 10b, b1). The upper cortical layers were much less myelinated than in area 8/FEF.

SMI-32ir was relatively high in area 45B (Figs. 11b, b1, c, c1, 12a, b, 13b, c), especially in the lower part of layer III, where immunopositive pyramids were relatively numerous and immunopositive apical dendrites were mostly confined. The lowest part of this layer displayed many quite large immunopositive pyramids (Figs. 12d, f, 13f, 14b), which may correspond to the large, darkly stained pyramids, observed in Nissl-stained material. In layer V, neuropil immunostaining was weaker than in area 8/FEF. This layer virtually lacked the large, darkly stained immunopositive pyramids, clearly evident in area 8/FEF and only sparse, small immunopositive cell bodies could be observed. The density of immunopositive pyramids in this layer (Fig. 14g) was significantly lower than that in area 8/FEF ($p < 0.001$).

Area 8r

Area 8r was identified in the caudalmost part of the prearcuate convexity cortex, at AP levels caudal to the tip of the PS, dorsal to area 45B (Fig. 3b, b1). Area 8r (Fig. 8d) was characterized, in general, by a relatively small overall thickness. Layer III was relatively thin, dense and homogeneous, layer IV was thin and difficult to demarcate and layer V was populated by densely packed small pyramids, only slightly larger in its ventral part. These features clearly distinguished this area from areas 45B (Fig. 15a) and 8/FEF (see, e.g., Fig. 6a). In rostral direction, area 8r extended, in all cases, at least as far as the caudal end of the PS, and, in several cases, also in the caudalmost part of this sulcus (Figs. 4a, 5a).

Area 8r was considerably less myelinated than areas 8/FEF and 45B (Fig. 9b) and characterized by relatively thin vertical bundles of fibers, a faint, but evident, outer band of Baillarger and a more densely labeled inner band of Baillarger (Fig. 10d, d1).

SMI-32 immunostaining was lower in area 8r than in areas 8/FEF and 45B, especially in layer III, mostly because of a much smaller amount of immunopositive apical dendrites (Figs. 11b, b1, 12a, b, 13a). Layer III pyramids (Figs. 13e, 14d) were relatively small, confined to the lower part of this layer. These cells appeared to be sparser than in areas 8/FEF and 45B, though no significant differences were observed in the quantitative analysis (Fig. 14g), likely because of the lower thickness of layer III in area 8r, with respect to areas 8/FEF and 45B. Layer V displayed a neuropil immunostaining denser than in area 45B and almost comparable to that observed in area 8/FEF and was populated by very small immunopositive cells. Their density (Fig. 12g) was higher than in all the other analyzed areas ($p < 0.001$), but 8/FEF.

Area 45A

Area 45A was identified rostral to area 8r on the caudal VPLF convexity cortex. Its major identifying cytoarchitectonic feature was the evident increase in cell size from the upper to the lower part of layer III, which, however, lacked the outstanding layer III pyramids typical of area 45B (Figs. 3c, c1, d, d1, 5b, c, 8c). This feature clearly distinguished this area from area 45B (Figs. 6b, c, 15b). Additional cytoarchitectonic features of area 45A (Fig. 8c) were a poorly defined layer II, a well-developed layer IV and a relatively dense layer V populated by small pyramids.

Area 45A was heavily myelinated (Figs. 9c, d, 10c, c1) and characterized by relatively thin and very close vertical bundles of fibers and a relatively high myelin content in the superficial layers. Both the outer and the inner bands of Baillarger were relatively thin, but quite evident. The outer band, however, was thicker and more labeled than the inner one.

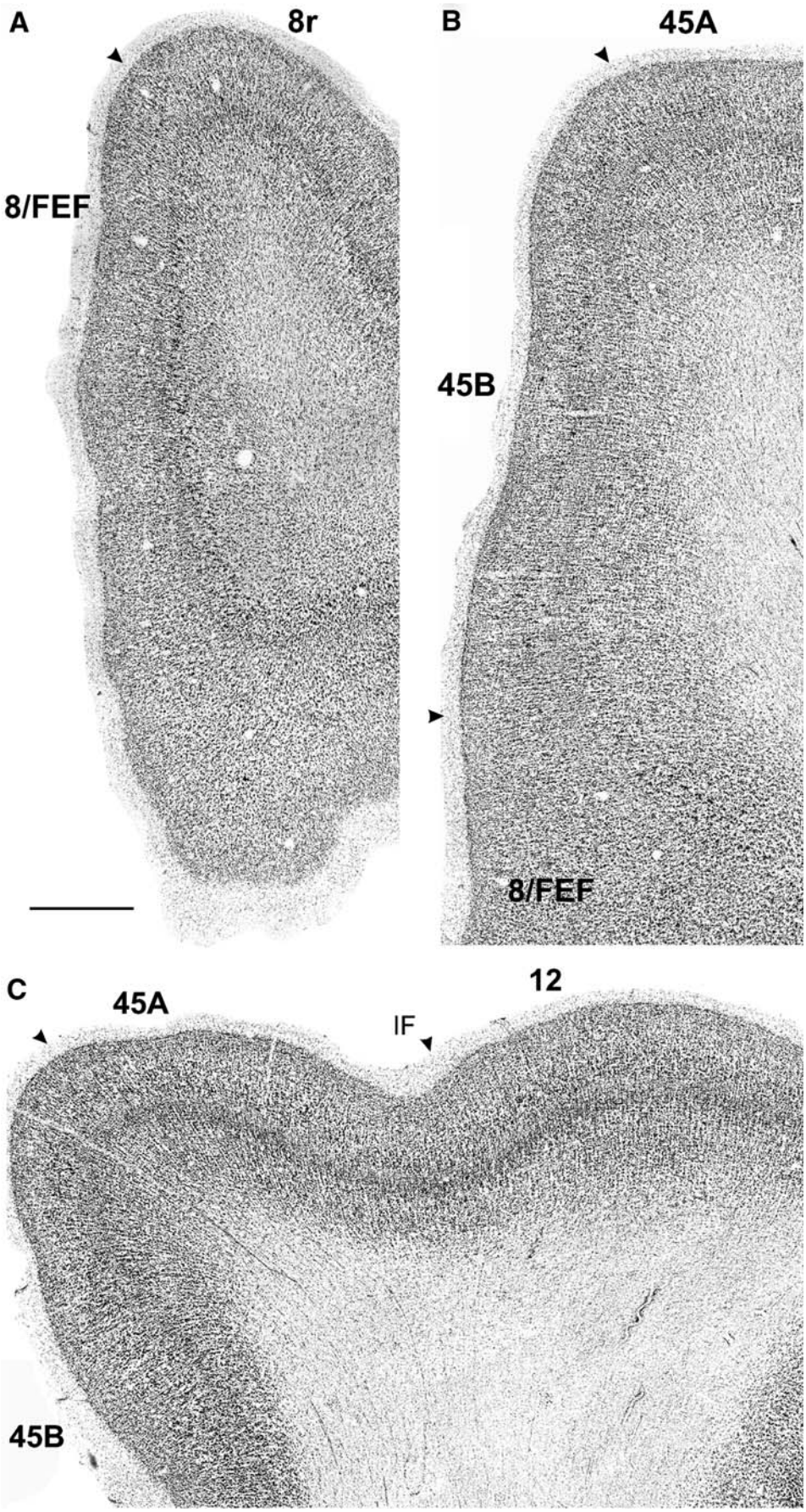

Fig. 6 Cytoarchitecture of the caudal VLPF. Higher magnification views of areas 8/FEF and 8r (**a**), 45B (**b**), and 45A and 12 (**c**). The location of the photomicrographs is indicated by *dashed boxes* in the sections shown in Fig. 5. *Arrows* mark the intermediate points of cytoarchitectonic transitions. *Scale bar* = 1 mm in **a** (applies to **a**–**c**)

SMI-32ir was very helpful for distinguishing area 45A from the dorsally adjacent area 46 and the ventrally and rostrally adjacent area 12 (Figs. 11c, c1, d, d1, 13b, c). In area 45A (Fig. 14c) layer III displayed dense, relatively small immunopositive pyramids, concentrated in lower layer III and immunopositive apical dendrites, in many cases ascending to more superficial layers. Quantitative analysis (Fig. 14g) showed that immunopositive layer III pyramids were denser than in the adjacent areas 45B ($p < 0.05$) and 46v ($p < 0.001$). In layer V, neuropil immunostaining was slightly denser than in area 45B. Immunopositive cell bodies were sparse, relatively small and less dense than in areas 8/FEF and 8r ($p < 0.001$).

Areas 46 and 12

Area 45A was completely located on the caudal VLPF convexity, extending rostrally as far as the IFS, when present. Dorsally, it bordered with the ventral part of area 46 (46v) at about 2–3 mm from the sulcal crest (Figs. 3c, c1, d, d1, 5b). Area 46v (Fig. 8e) was characterized by a thin, but evident, layer II and a cell dense layer III almost homogeneously populated by relatively small pyramids, which distinguished this area from area 45A (Fig. 15c). Layer IV was well developed and cell dense and layer V was densely populated by small pyramids. Layer VI, was rather homogeneous in the proximity of the border with area 45A, but showed an evident sublamination within the lower bank of the PS. Except for this different layer VI organization, area 46v appeared cytoarchitectonically quite homogeneous as far as the fundus of the PS.

Myelin staining was relatively light (Fig. 9c, d) in area 46v, which clearly distinguished it from area 45A. In particular, the vertical bundles of fibers were dense, but very fine-caliber and both bands of Baillarger were evident, but lightly labeled (Fig. 10e, e1).

SMI-32ir was considerably lower in area 46v than in areas 45A (Figs. 11c, c1, d, d1, 13b) and 8r (Fig. 12a, b). In layer III immunopositive apical dendrites were relatively poor and immunopositive pyramids relatively sparse and small (Fig. 14e). The density of these cells was the lowest among all the analyzed areas and significantly different from all areas ($p < 0.001$), but 45B (Fig. 14g). An evident band of immunopositive neuropil was observed in layer V which was very poor in immunopositive cell bodies.

Rostral to area 45B, area 45A was bordered ventrally by a sector of area 12 (Fig. 3d, d1), which appears to correspond well to area 12l of Carmichael and Price (1994). This border run almost obliquely from the rostral end of the IAS in rostro-dorsal direction. This area 12 sector displayed a size gradient in layer III, in which, however, layer IIIc pyramids were considerably smaller than in area 45A (Figs. 6c, 15d). Additional cytoarchitectonic features were a relatively thick layer I, a thin, but evident layer II, a well developed layer IV and a sublaminated layer V with somewhat larger pyramids in layer Vb (Fig. 8f).

The myeloarchitecture of area 12 was similar to that of area 45A and characterized by thin and close vertical bundles of fibers and by evident outer and inner bands of Baillarger (Fig. 10f, f1). However, the overall myelin staining was, in general, lighter than in area 45A.

In SMI-32 immunostained material, area 12 (Figs. 11d, d1, 13h, 14f) presented, in layer III, small, sparse, but darkly stained, pyramids in the lowest part and a very low content of immunopositive apical dendrites in the lower half. In the infragranular layers, neuropil immunostaining tended to be fainter than in area 45A.

Rostral to area 45A (Fig. 3e, e1) the cortical convexity was occupied dorsally by area 46v and ventrally by an area with cytoarchitectural characteristics similar to those of area 12. In SMI-32 immunostained material this more rostral part of area 46v (Fig. 11e1) displayed a gradual decrease in overall immunostaining intensity, without any clear chemoarchitectonic border. In contrast, an increase in SMI-32ir was observed, more evident in coronal sections from Case 12r (Fig. 11e1), in this more rostral area 12 sector, possibly corresponding to area 12r of Carmichael and Price (1994), characterized by the presence of numerous darkly stained cell bodies in the lower part, a very low content of immunopositive apical dendrites and a very weak immunostaining in the infragranular layers.

Distribution of CBir in the caudal VLPF

Figure 16a–e, shows representative CB immunostained fields of areas 8/FEF, 45B, 8r, 45A, and 46v. In general, the distribution pattern of CBir was quite similar all over the caudal VLPF, lacking any sharply distinguishable chemoarchitectonic border. Nevertheless, some differences were observed, at a qualitative level of analysis, which allow one, first of all, to distinguish two main caudal VLPF regions, a caudal one, including areas 8/FEF, 45B, and 8r and a rostral one, including areas 45A and 46v. In areas 8/FEF, 45B, and 8r (Fig. 16a, b, c) the darkly stained non-pyramidal cells were highly concentrated in layer II and in the uppermost part of layer III, where immunopositive neuropil was densely stained. These cells were much sparser in the remaining part of layer III, especially in area 8/FEF, rare in layer IV and very sparse in layers V and VI. Neuropil staining in these layers was quite weak except for a faint band of immunopositive neuropil in layer V. In

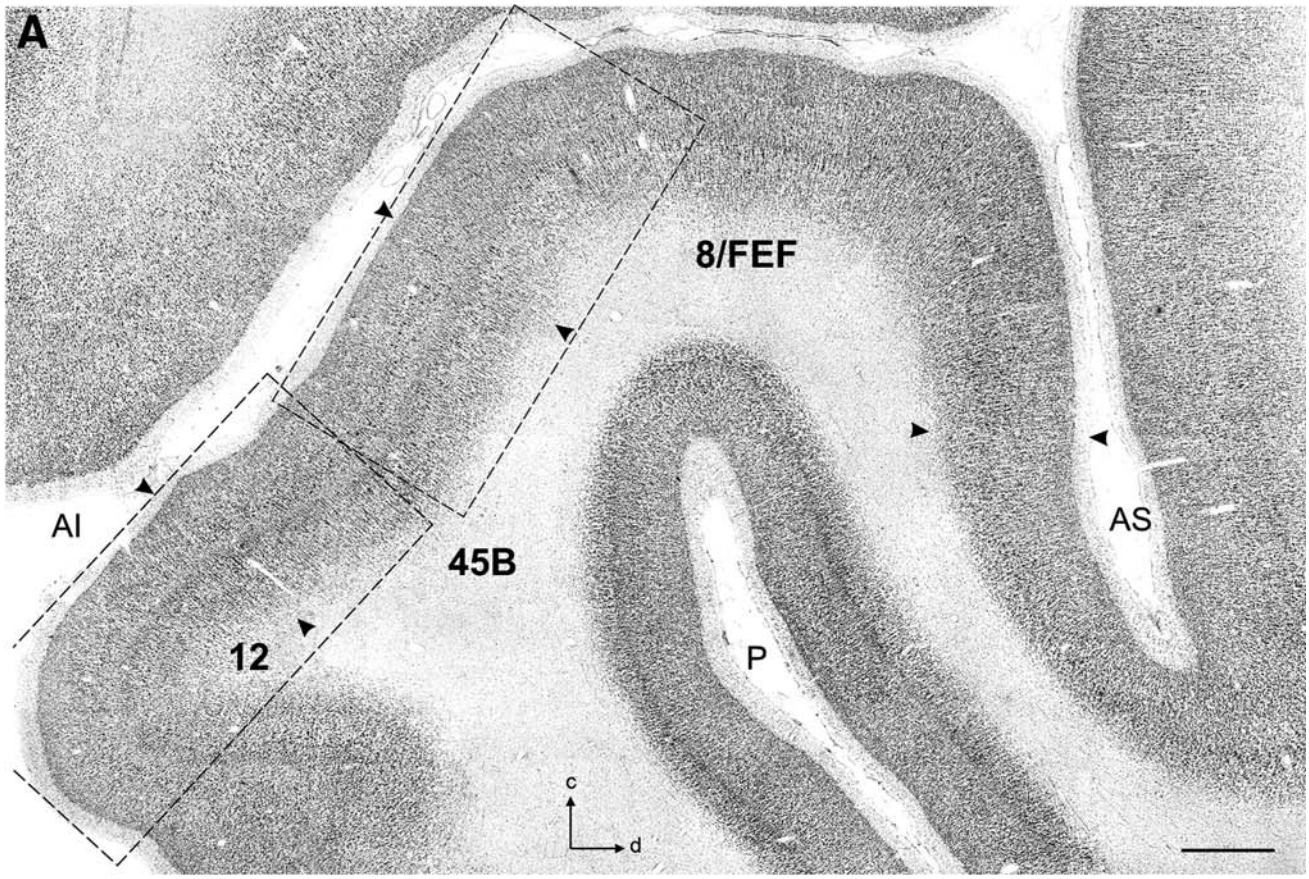
A
8/FEF
AI
45B
12
P
AS
c
d

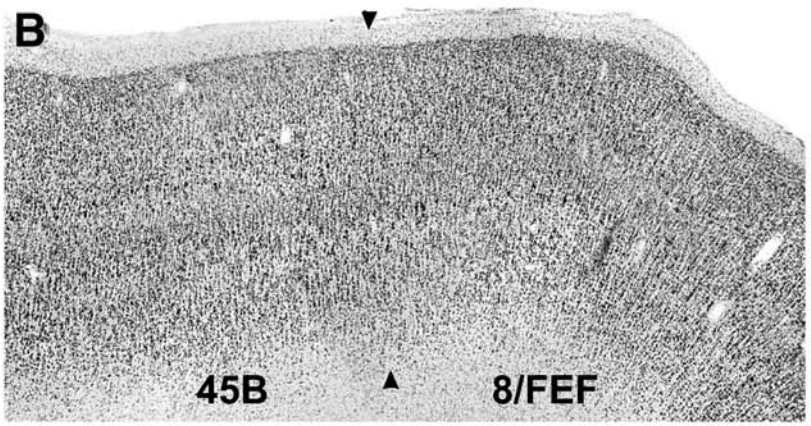
B
45B
8/FEF

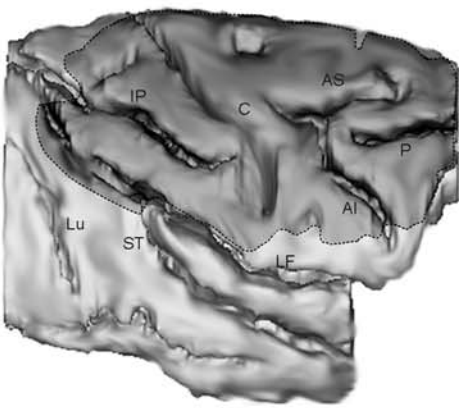
IP
C
AS
P
AI
Lu
ST
LF

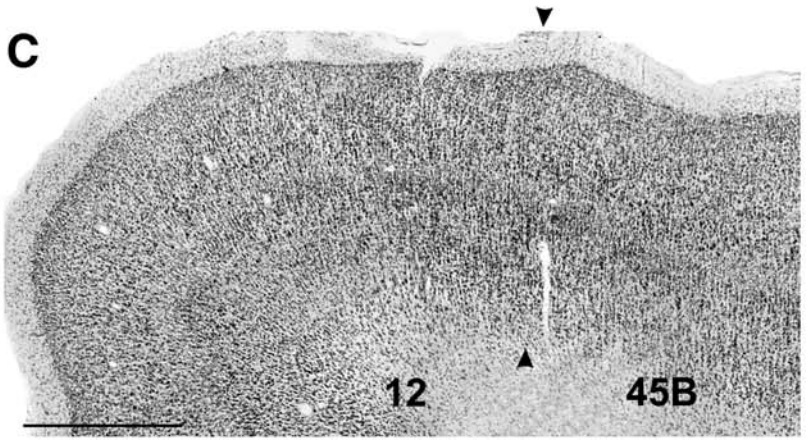
C
12
45B

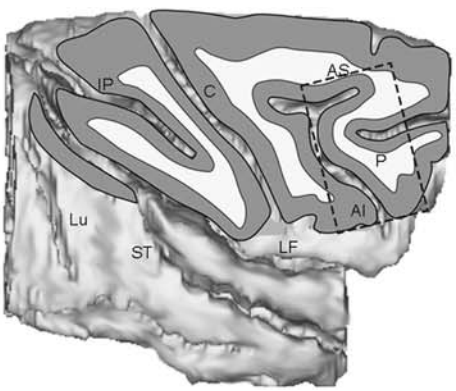
IP
C
P
AI
Lu
ST
LF

◀ **Fig. 7** Cytoarchitecture of the caudal VLPF. **a** Low-power photomicrograph of a Nissl-stained tangential to the arcuate sulcus section, taken from Case PR18. The upper 3D reconstruction of a *right hemisphere* shows in *darker grey* the brain sector dissected in order to expose the approximate level of the section, shown in the lower 3D reconstruction. The *dashed box* on the reconstruction indicates the locations of the photomicrograph. *Scale bar* = 1 mm. **b** Higher magnification view of the cytoarchitectonic transitions between areas 8/FEF and 45B. **c** Higher magnification view of the cytoarchitectonic transitions between areas 45B and 12. The location of the photomicrographs is indicated by the *dashed boxes* on the section shown in **a**. *Scale bar* = 1 mm in **c** (applies also to **b**). Conventions and abbreviations as in Figs. 1 and 3

contrast, both areas 45A and 46v (Fig. 16d, e) were characterized by a much higher overall CB immunostaining. Darkly stained nonpyramidal cells, though highly concentrated in the most superficial layers, were very numerous, though with some variability across cases, through the entire extent of layer III, where immunopositive neuropil was quite densely stained. Furthermore, both these areas displayed a relatively higher concentration of darkly stained immunopositive cells in layer V, where a band of neuropil, denser than in areas 8/FEF, 45B, and 8r was clearly visible even at low power view. A similar pattern of CBir was observed rostral to area 45A, in areas 46v and 12. In contrast, in the area 12 sector ventral to area 45A, CB immunostaining was much stronger and similar to that observed in the orbitofrontal cortex. A small population of CB immunopositive pyramidal cells was identified in all the studied areas. These cells, virtually all lightly stained, were relatively more frequently encountered in area 45A.

The quantitative analysis of the density of CB immunopositive nonpyramidal and pyramidal neurons in each of the five studied areas confirmed the general subdivision of the caudal VLPF into a caudal and a rostral neurochemically different region.

A two-way ANOVA for repeated measures showed a significant main effect of both Cell type [$F(1;17) = 15627$, $p < 0.001$] and Area [$F(4;68) = 95.398$, $p < 0.001$] and a significant interaction effect (Cell type × Area) [$F(4;68) = 45.359$, $p < 0.001$]. With respect to the density of nonpyramidal immunopositive cell (Fig. 17a), post hoc analysis showed that: (a) the density in areas 45A and 46v was significantly higher (about 20%) than that in areas 8/FEF, 45B, and 8r ($p < 0.001$); b) the relatively small difference between areas 45B and 8r (about 5%) was significant ($p < 0.05$). With respect to the density of immunopositive pyramidal cells (Fig. 17b), the post hoc analysis revealed that: (a) the density in area 45A, where they represented about 10% of the whole population of CB immunopositive cells, was significantly higher than in areas 8/FEF and 45B ($p < 0.001$); (b) the density in area 8/FEF was significantly lower than in areas 8r, 45A, and 46v ($p < 0.001$).

The two-way ANOVA performed on the values of laminar density of CB immunopositive nonpyramidal cells showed a significant main effect of Area [$F(4;68) = 27.083$, $p < 0.001$] and Layer/Sublamina [$F(5;85) = 475.63$, $p < 0.001$] and a significant interaction effect (Area × Layer/Sublamina) [$F(20;340) = 6.5724$, $p < 0.001$]. In spite of a general similarity across the five studied areas, some significant differences were observed in the second sublamina of layer II/III and in layer V (Fig. 17c). In the second sublamina of layer II/III, post hoc analysis showed that the density in areas 8r, 45A, and 46v was higher than in areas 8/FEF and 45B ($p < 0.001$). This difference was evident also at a qualitative level of analysis (Fig. 17d, e). In layer V the density in areas 45A and 46v was higher than in areas 8/FEF ($p < 0.001$ and $p < 0.01$, respectively).

All together, these data indicated that areas 8/FEF and 45B are different from areas 45A and 46v in terms of both general and laminar (second layers II/III sublamina) density of CB immunopositive nonpyramidal cells. Moreover, area 8r was similar to areas 8/FEF in terms of overall density and differed from areas 8/FEF and 45B in the laminar distribution in the second sublamina of layers II/III.

Location and extent of areas 8/FEF, 8r, 45B, and 45A

Table 2 summarizes the major architectonic features recognized and successfully used for the identification of the above-described caudal VLPF areas in all the examined hemispheres, independently of the macaque species used.

To obtain an estimate of the distribution of these areas, a 3D reconstruction was generated from the individual sections for each case studied. The location and the extent of areas 8/FEF, 8r, 45B and 45A are shown in two reconstructed hemispheres (Cases 18r and 12r) in Fig. 18a. For each hemisphere, the frontal lobe is shown from a dorsolateral view and from a caudolateral view in which the anterior bank of the IAS was exposed with dissection of the 3D reconstruction along the fundus of the arcuate sulcus. Both location and extent of the four areas are quite consistent and the areal distribution was very similar in the rest of the cases studied.

Moreover, in order to have an estimate of the interindividual variability in location and extent of the identified areas, 2D reconstructions of the frontal lobe and of the identified architectonic areas of ten hemispheres have been warped to fit with an "average" frontal lobe. Panels B1–B4 in Fig. 18b show the degree of overlap of the ten architectonic maps, separately for each area. In each panel, the cortical surface where at least nine individual maps overlapped is shown in red, while that occupied by no more

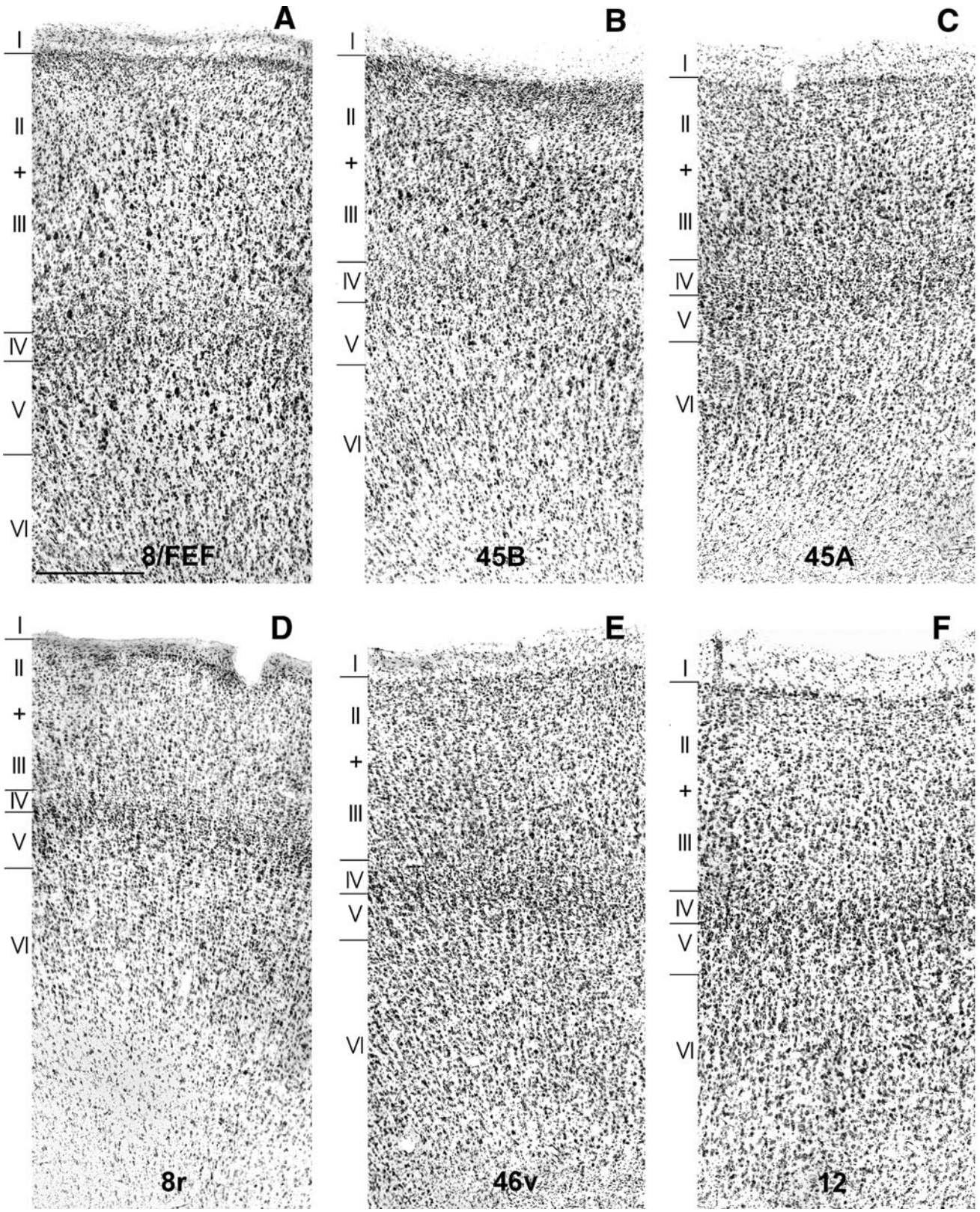

Fig. 8 Cytoarchitecture of the caudal VLPF. Higher power photomicrographs of representative fields of cytoarchitectonic areas 8/FEF (**a**), 45B (**b**), 45A (**c**), 8r (**d**), 46v (**e**), and 12 (**f**), taken from Case 12r. The location of all the photomicrographs, but that in **a**, is indicated by *dashed boxes* in Fig. 2b1, d1. The photomicrograph of area 8/FEF has been taken from a section 600 μm rostral to that shown in Fig. 2a1. *Scale bar* = 500 μm in **a** (applies to **a**–**f**)

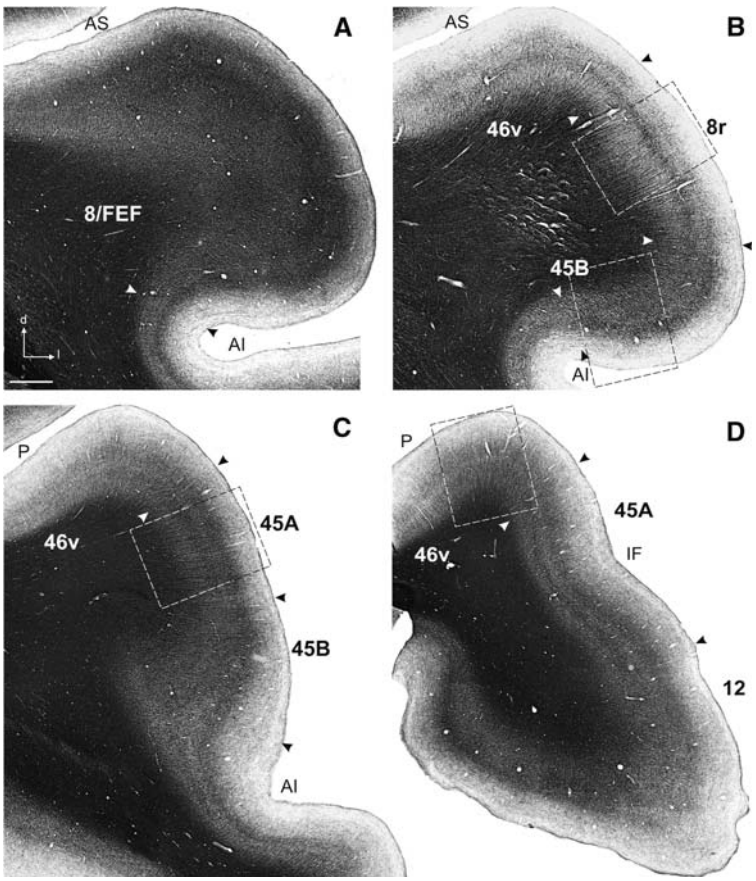

Fig. 9 Myeloarchitecture of the caudal VLPF. **a–d** Low-power photomicrographs of a series of myelin-stained coronal sections, in a caudal to rostral order, taken from Case 29r at AP levels comparable to the sections taken from Case 12r, shown in Fig. 2a1–d1. *Arrows* on the photomicrographs indicate the location of cytoarchitectonic borders reported from adjacent Nissl-stained sections. *Dashed boxes* indicate the location of the higher magnification views of Fig. 10b–e. *Scale bar* = 1 mm in **a** (applies to **a**–**d**). Section orientation in **a** applies to **a**–**d**. Abbreviations as in Figs. 1, 2, and 3

than two of them is shown in blue. In panel B5, the cortical surfaces occupied by areas 8/FEF, 8r, 45B, and 45A in at least nine maps and in at least seven maps (the areal *core*) are shown in red and orange, respectively. These data indicate that, in spite of some interindividual variability, the location and the extent of these areas was quite similar across different cases and species.

All together, the 2D and 3D reconstructions of Fig. 18 thoroughly describe the brain location and extent of areas 8/FEF, 8r, 45B and 45A, as well as their relationships with neighboring cortical areas. A few points are worth noting: (a) in agreement with Stanton et al. (1989), area 8/FEF is limited to the prearcuate cortex and the crest of the arcuate sulcus. The ventral border of its *core* is located at about 53% of the total length of the IAS; (b) area 8r extends for about 9 mm in dorso-ventral direction and 2–3 mm in rostro-caudal direction, always reaching the tip of the PS and, in many cases, occupying the caudalmost part of this sulcus; (c) the *core* of area 45B extends for about 4–5 mm along the anterior bank of the IAS and does not include its very ventralmost part; (d) the *core* of area 45A extends for about 6 mm in dorso-ventral direction and about 4 mm in rostro-caudal direction, reaching the caudal part of the IFS, which can be considered as a macroscopic landmark for the rostral border of this area. It should be noted however, that an evident IFS was observed only in about 70% of the hemispheres used for the generation of the average hemisphere, without any bias in favor of one of the two macaque species used for this purpose.

Discussion

In the present study we have provided a detailed description of the architectonic organization of the caudal VLPF of the macaque monkey by using a combination of cyto-, myelo-, and chemoarchitectonic criteria. In this way, we have defined several architectonically distinct areas, completely or only partially located in the caudal VLPF. Two of these areas—8/FEF and 45B—are almost completely buried in the anterior bank of the IAS. Area 8/FEF occupies about the dorsal half of this bank, extending also dorsally in the superior prearcuate bank, while area 45B occupies virtually the entire extent of the ventral half of it. Two other areas—8r and 45A—are located on the VLPF convexity cortex. Area 8r occupies the caudalmost part of both the dorsal and the ventral prearcuate convexity cortex, extending rostrally as far as the caudalmost part of the PS. Area 45A occupies most of the cortical convexity located

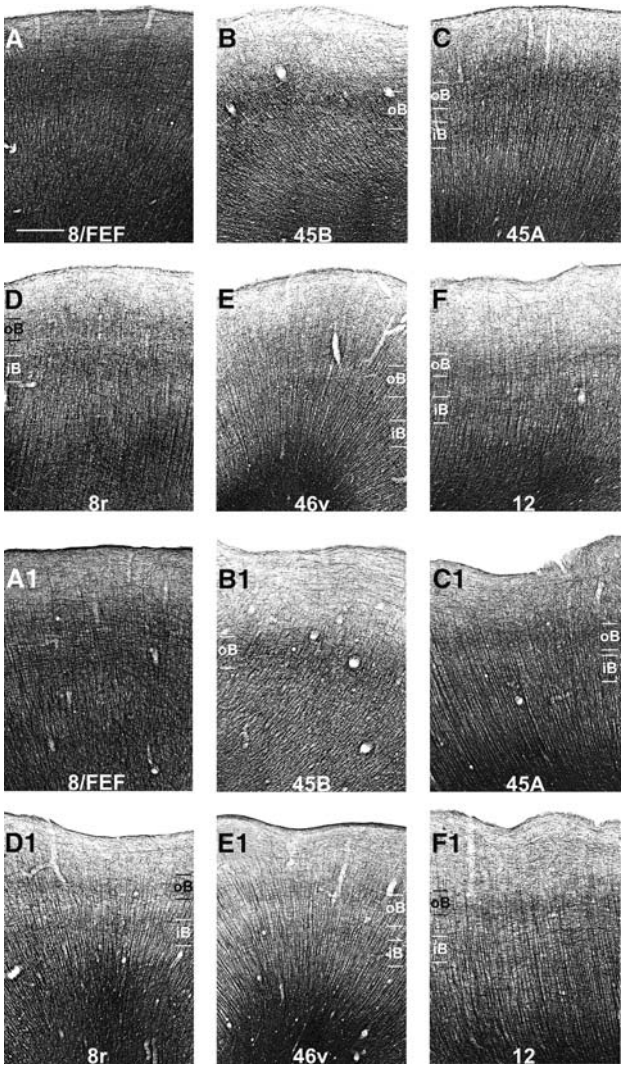

Fig. 10 Myeloarchitecture of the caudal VLPF. Higher magnification views of representative myeloarchitectonic fields of areas 8/FEF (**a**), 45B (**b**), 45A (**c**), 8r (**d**), 46v (**e**), and 12 (**f**), taken from Case 29r. The location of **b**–**e**, is indicated by *dashed boxes* in Fig. 9b–d. The fields shown in **a** and **f** are from sections close to those shown in Fig. 9a and d, respectively. Higher magnification views of representative myeloarchitectonic fields of areas 8/FEF (**a1**), 45B (**b1**), 45A (**c1**), 8r (**d1**), 46v (**e1**), and 12 (**f1**), taken from Case 38. *iB* inner stria of Baillarger, *oB* outer stria of Baillarger. *Scale bar* = 500 μm in **a** (applies to all photomicrographs)

between the IAS and the PS, extending rostrally as far as the IFS. Finally, area 45A borders dorsally with area 46v, which extends up to the fundus of the PS, and ventrally with area 12, which extends into the lateral part of the orbitofrontal cortex.

The present data, showing the existence of two distinct prearcuate convexity areas—8r and 45A—extend other architectonic subdivisions of the caudal VLPF and provide a new multiarchitectonic frame of reference for this prefrontal region.

Architectonics of the caudal VLPF

The entire extent of the prearcuate bank and of the adjacent convexity cortex was originally considered by Brodmann (1905) as a single cytoarchitectonic area, designated as area 8. A different subdivision of the macaque prefrontal cortex was subsequently proposed by Walker (1940), so far followed by most of the electrophysiological and connectional studies of this region. In Walker's map the prearcuate bank is made up of a dorsal and a ventral area, designated as 8A and 45, respectively, extending onto the prearcuate convexity and replaced rostrally by prefrontal area 46. Although using different nomenclatures, von Bonin and Bailey (1947), Barbas and Pandya (1989) and Preuss and Goldman-Rakic (1991) basically agreed with the dorso-ventral subdivision of Brodmann's area 8, or at least of the prearcuate bank, proposed by Walker (1940).

The discovery of a functionally distinct frontal eye field—the FEF—located in the prearcuate cortex (Bruce and Goldberg 1984; Bruce et al. 1985), seriously challenged the possible functional validity of these architectonic subdivisions. In fact, the FEF, defined as the cortical sector from which eye movements can be evoked with low-current intracortical microstimulation, is confined to the caudalmost part of both the superior and inferior prearcuate bank. Accordingly, this field would not have an architectonic counterpart, partially overlapping with both the ventral and the dorsal subdivisions of the prearcuate bank (e.g., areas 8A and 45 of Walker). This issue was successfully addressed by Stanton et al. (1989) in a combined functional and cytoarchitectonic study. This study showed that the FEF corresponds to a distinct cytoarchitectonic field, characterized by the presence of large layer V pyramids, limited to the prearcuate bank and straddling over the caudal parts of Walker's areas 8A and 45. Thus, as far as the caudal VLPF is concerned, these data clearly demonstrated that Walker's area 45 is not homogeneous.

Petrides and Pandya (1994, 1999, 2002) have readdressed the issue of the organization of the caudal VLPF in a series of cytoarchitectonic studies. These authors agreed with Stanton et al. (1989) that the dorsal part of Walker's area 45 corresponds to the ventral part of the FEF (Cadoret et al. 2000). This field—area 8Av—was, however, extended onto the convexity cortex as far as the caudal tip of the PS. Ventral to area 8Av, Petrides and Pandya (1994, 2002) identified a cytoarchitectonic area displaying very large layer III pyramids, a well developed layer IV and lacking large layer V pyramids. This area—area 45—occupies the ventral part of the prearcuate bank, and the convexity cortex rostral to area 8Av. The anterior part of this area was designated as area 45A, while the posterior part, lying in the prearcuate bank was designated as area 45B. Accordingly, area 45 as defined by Petrides and Pandya (1994,

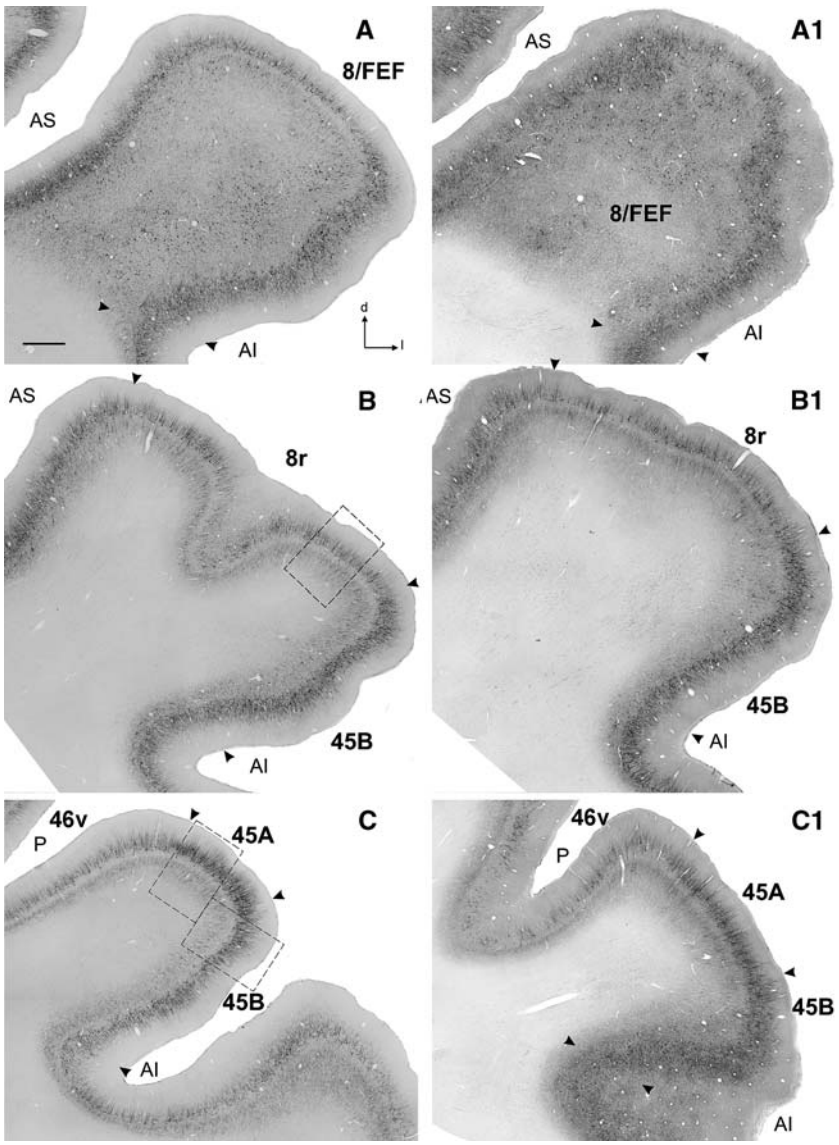

Fig. 11 Distribution of SMI-32ir in the caudal VLPF. **a–d** Low-power photomicrographs of a series of SMI-32 immunostained coronal sections, in a caudal to rostral order, taken from Case 18r. Section in **a** is adjacent to that shown in Fig. 3a. Sections in **b**, **c**, and **d** are close to those shown in Fig. 3b, c, and d, respectively. **a1–e1** Low-power photomicrographs of a series of SMI-32 immunostained coronal sections, in a caudal to rostral order, taken from Case 12r. Sections in **a1** and **b1** are adjacent to those shown in Fig. 3a1 and b1, respectively. Sections in **c1**, **d1**, and **e1** are close to those shown in Fig. 3c1, d1, and e1, respectively. No material was available for case 18r at the level shown in **e1** for Case 12r. *Arrows* on the photomicrographs indicate the location of cytoarchitectonic borders reported from Nissl-stained sections. *Scale bar* = 1 mm in **a** (applies to all photomicrographs). Section orientation in **a**, applies to all photomicrographs. *Dashed boxes* in **b–d** indicate the location of the higher magnification views of Fig. 12. Abbreviations as in Figs. 1, 2, and 3

2002), is a completely newly defined area, which, in the prearcuate bank, corresponds only to the ventral part of area 45 of Walker (1940). Moreover, onto the caudal VLPF convexity, this area occupies a cortical sector of highly controversial architectonic attribution, considered by Walker (1940) as part of area 46, by Barbas and Pandya (1989) as part of areas ventral 8 and 46 and by Preuss and Goldman-Rakic (1991) as part of area 8Ar, 12 and, possibly, 46.

The present data strongly support the architectonic distinctiveness of a caudal VLPF sector—area 45—with respect to areas 8, 46, and 12, in agreement with Petrides and Pandya (1994, 2002), but also provide robust, multimodal evidence that area 45 is made up of two distinct architectonic areas, designated as areas 45A and 45B. In this respect, it should be noted that a similar subdivision of area 45 was already set by Petrides and Pandya (1994, 2002). These authors, however, did not describe the criteria used for distinguishing these two sectors and, from their cytoarchitectonic and connectional studies, it seems quite clear that area 45, as a whole, was considered as a single architectonic entity.

In Nissl-stained material, we found that the evident size gradient in layer III and the virtual lack of very large and deeply stained layer III pyramids clearly distinguished area 45A from area 45B. In spite of some interindividual variability, these cytoarchitectonic differences have been constantly and reliably observed in all hemispheres analyzed in the present study, including hemispheres from different monkey species and cut along different planes of sectioning. Although it is possible that architectonic differences between areas 45A and 45B were noticed by Petrides and Pandya (1994, 2002), but not considered as a reliable and sufficient criterion for setting a cytoarchitectonic border, in the present

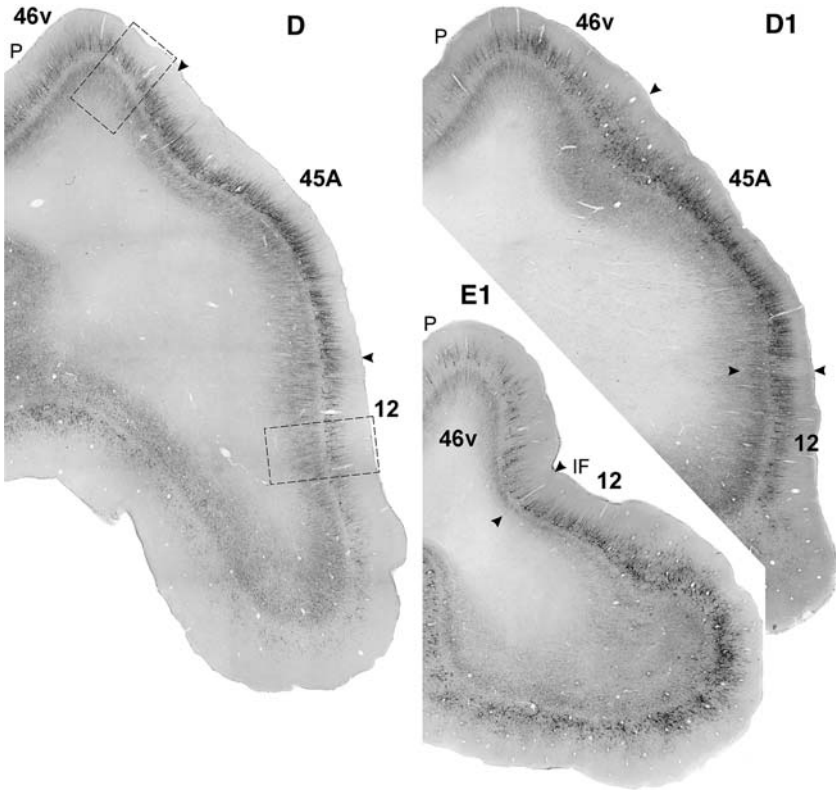

Fig. 11 continued

study we provided independent architectonic evidence in favor of the distinctiveness of these two areas.

First, in myelin-stained sections, although both areas 45A and 45B are relatively heavily myelinated, an evident inner band of Baillarger clearly distinguished area 45A from area 45B. A myeloarchitetonic sector corresponding to area 45A was not recognized by Preuss and Goldman-Rakic (1991), likely because of its myeloarchitectural pattern relatively similar to that of area 12. In a previous study, however, Preuss and Goldman-Rakic (1989) have suggested that a myeloarchitectonic field, likely corresponding to area 45A, could represent an additional subdivision of area 46 or area 12.

Second, our chemoarchitectonic data further support the presently proposed subdivision. In particular, SMI-32ir was very helpful for a clear definition of area 45A, relatively rich in immunopositive pyramids and dendrites in layer III, against areas 46 and 12, where cells and dendrites immunostaining is considerably poorer. Furthermore, although similar in their general pattern of SMI-32ir, areas 45A and 45B differed in terms of density and size of layer III immunopositive pyramids and in terms of density and laminar distribution of layer III immunopositive dendrites. Finally, areas 45A and 45B showed significant differences in their distribution patterns of CB immunopositive nonpyramidal cells, suggesting the existence of a different organization of the intrinsic cortical circuitry in these two areas, as well as of CB immunopositive pyramids. In this respect, it is interesting to note that, on the basis of the absolute number and laminar distribution of CB immunopositive nonpyramidal cells, area 45A appears quite similar to area 46v area, while 45B appears quite similar to area 8/FEF.

As Stanton et al. (1989) and Petrides and Pandya (1994, 1999, 2002), we also found clear evidence for setting an architectonic border at about half of the ventral prearcuate bank and were able to define a distinct architectonic field—area 8/FEF—which appears to exactly correspond to the FEF as defined by Stanton et al. (1989). Furthermore, although this area displays a gradient in the number and size of layer III pyramids from the dorsal to the ventral part, in agreement with Stanton et al. (1989) we did not find consistent changes, which could justify a dorso-ventral subdivision of this field. Finally, the ventral border of area 8/FEF was set in a location closely corresponding to the ventral border of the FEF (Stanton et al. 1989) or of area 8Av of Petrides and Pandya (1994, 2002). The present data extend the observation of these authors in providing additional, independent myelo- and chemoarchitectonic criteria useful for the localization of this border.

Finally, a further major finding of the present study has been the definition of a distinct architectonic area—8r—lying onto the caudalmost prearcuate convexity cortex, rostral to area 8/FEF and caudal to area 45A. In this

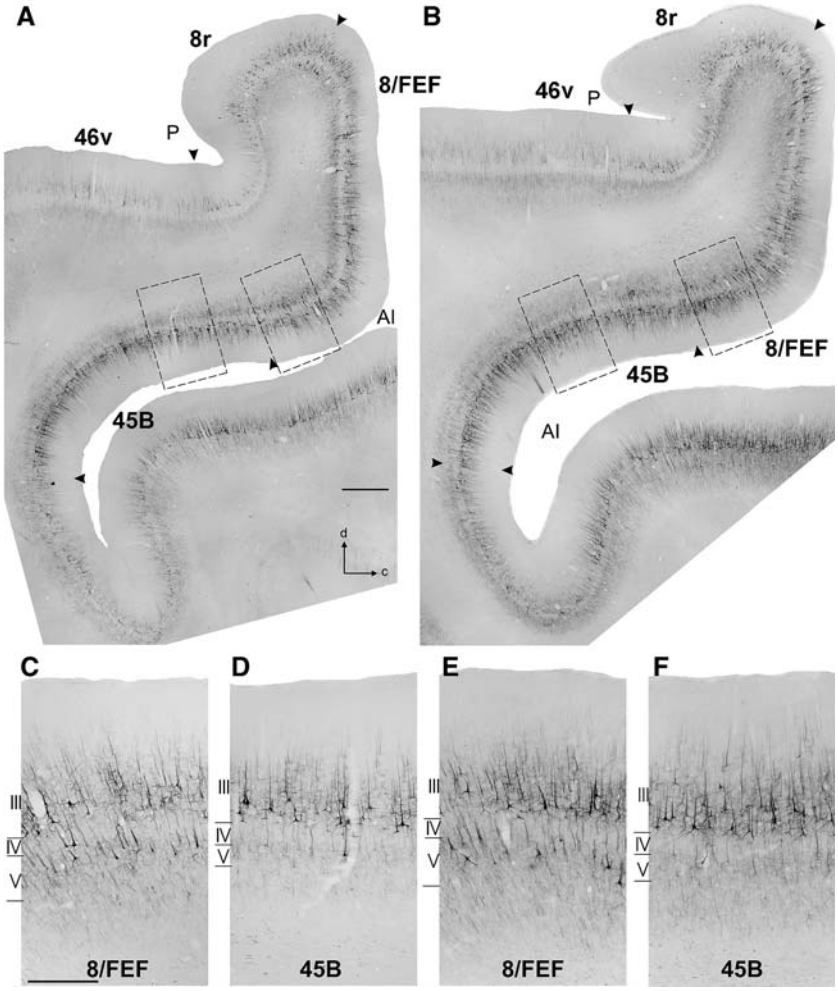

Fig. 12 Distribution of SMI-32ir in the caudal VLPF. **a** Low-power photomicrograph of a SMI-32 immunostained parasagittal section taken from Case M4l, at a level close to that shown in Fig. 4a. **b** Low-power photomicrograph of a SMI-32 immunostained parasagittal section taken from Case M3 at a level slightly medial to that shown in **a** and shown as a *left hemisphere*. *Arrows* on the photomicrographs indicate the location of cytoarchitectonic borders reported from adjacent Nissl-stained sections. *Scale bar* = 1 mm in **a** (applies also to **b**). Section orientation in **a**, applies also to **b**. *Dashed boxes* in **a** indicate the location of the higher magnification views shown in **c** and **d**. *Dashed boxes* in **b** indicate the location of the higher magnification views shown in **e** and **f**. Higher magnification views of areas 8/FEF (**c**) and 45B (**d**) taken from the section shown in **a**. Higher magnification views of areas 8/FEF (**e**) and 45B (**f**) taken from the section shown in **b**. *Scale bar* = 500 μm in **c** (applies to **c**–**f**). Abbreviations as in Figs. 1 and 2

respect, it should be noted that Preuss and Goldman-Rakic (1991) were able to define in myeloarchitectonic material an area—8Ar—which appears to largely overlap with area 8r of the present study. Furthermore, in a recent study based on unbiased stereological analysis (Medalla and Barbas 2006) the prearcuate bank and the prearcuate convexity were found to differ in terms of overall neuronal density. In the present study, we confirm and extend these observations, providing multiarchitectonic evidence in favor of the architectonic distinctiveness of this prearcuate sector. This finding fits well with the observations of Stanton et al. (1989) that the FEF, as cytoarchitectonically and functionally defined, do not extend onto the prearcuate convexity for more than 1–2 mm.

Functional considerations

The present study indicates that the architectonic organization of the macaque caudal VLPF is more complex than that proposed in other architectonic studies. The possible functional validity of the presently proposed subdivision is an issue that certainly needs to be addressed in future studies, in which connectional and electrophysiological data are correlated with architectonics. Nevertheless, the present data appear quite promising in clarifying some apparently controversial data related to the connectional and functional organization of area 45 and of the caudalmost prearcuate convexity.

Until its identification by Petrides and Pandya (1994), no studies have specifically focused on the connectional and functional properties of area 45. In fact, likely because of its controversial architectonic definition, most of the cortical sector corresponding to area 45A has been commonly considered, in the functional literature, as part of a larger VLPF region, mostly overlapping with Walker's area 12, playing a role in object and faces encoding in working memory (Wilson et al. 1993; O Scalaidhe et al. 1997, 1999; Levy and Goldman-Rakic 2000) or in conditional learning based on object identity (Passingham 1993; Passingham et al. 2000). Furthermore, very likely for the same reasons, connectional studies have been mostly focused on area 12

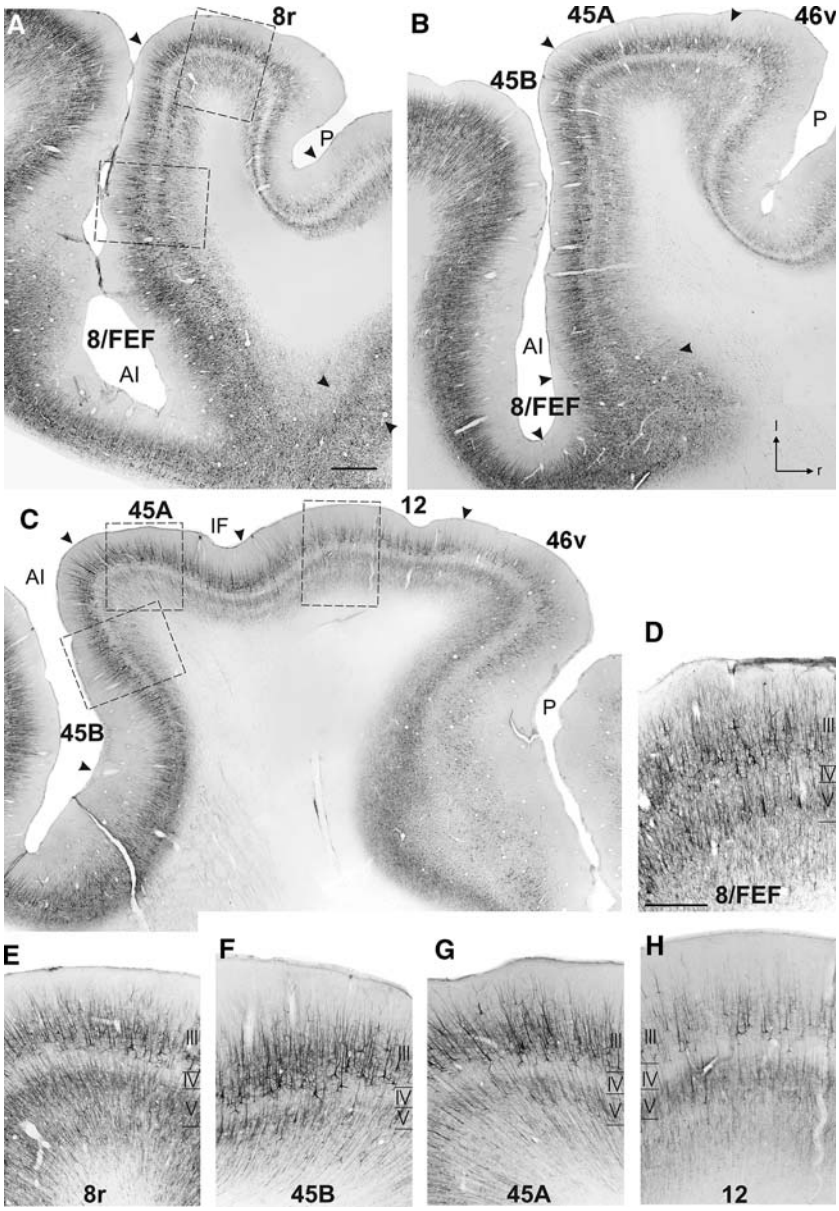

Fig. 13 Distribution of SMI-32ir in the caudal VLPF. **a–c** Low-power photomicrographs of SMI-32 immunostained perpendicular to the IAS sections, in a dorsal to a ventral order, taken from Case PR17, adjacent or close to the sections shown in Fig. 5. *Arrows* on the photomicrographs indicate the location of cytoarchitectonic borders reported from adjacent Nissl-stained sections. *Scale bar* = 1 mm in **a** (applies to **a–c**). Section orientation in **b** (applies to **a–c**). *Dashed boxes* indicate the locations of the of the higher magnification views shown in **d–h**. Higher magnification views of representative fields of areas 8/FEF (**d**), 8r (**e**), 45B (**f**), 45A (**g**), and 12 (**h**), taken from the sections shown in **a–c**. *Scale bar* = 500 μm in **d** (applies to **d–h**). Abbreviations as in Figs. 1, 2, and 3

and its subdivisions (e.g., Barbas 1988; Barbas and Pandya 1989; Carmichael and Price 1995a, b) or on area 46 (Barbas and Mesulam 1985; Barbas 1988; Preuss and Goldman-Rakic 1989). Petrides and Pandya (2002) provided the first description of the cortical connectivity of area 45 on the basis of relatively large tracer injections, likely involving both areas 45A and 45B, considered, as mentioned above, all together as a single area. Their results showed that area 45 is a target of rich projections originating from auditory-related areas of the STG and from multimodal areas of the upper bank of the superior temporal sulcus (area STP). These observations were considered by Petrides and Pandya (2002) as a strong argument in favor of the notion, based also on comparative cytoarchitectonic analysis, that the monkey area 45 is the possible homolog of the corresponding area of the human brain, that, in the left hemisphere, corresponds to the rostral part of the Broca's region (see also Petrides 2005). This hypothesis found strong support in electrophysiological studies (Romanski and Goldman-Rakic 2002; Romanski et al. 2005; Sugihara et al. 2006) showing that area 45 contains neurons responsive to auditory, visual or combined auditory and visual communication stimuli, suggesting an integration, in this area, of communicative information from the auditory and the visual domains.

The study of Petrides and Pandya (2002), however, showed that area 45 displays strong connections also with different subdivisions of area 8, including the FEF and with a rostral sector of the dorsal premotor cortex, likely corresponding to SEF. Considering that in humans the

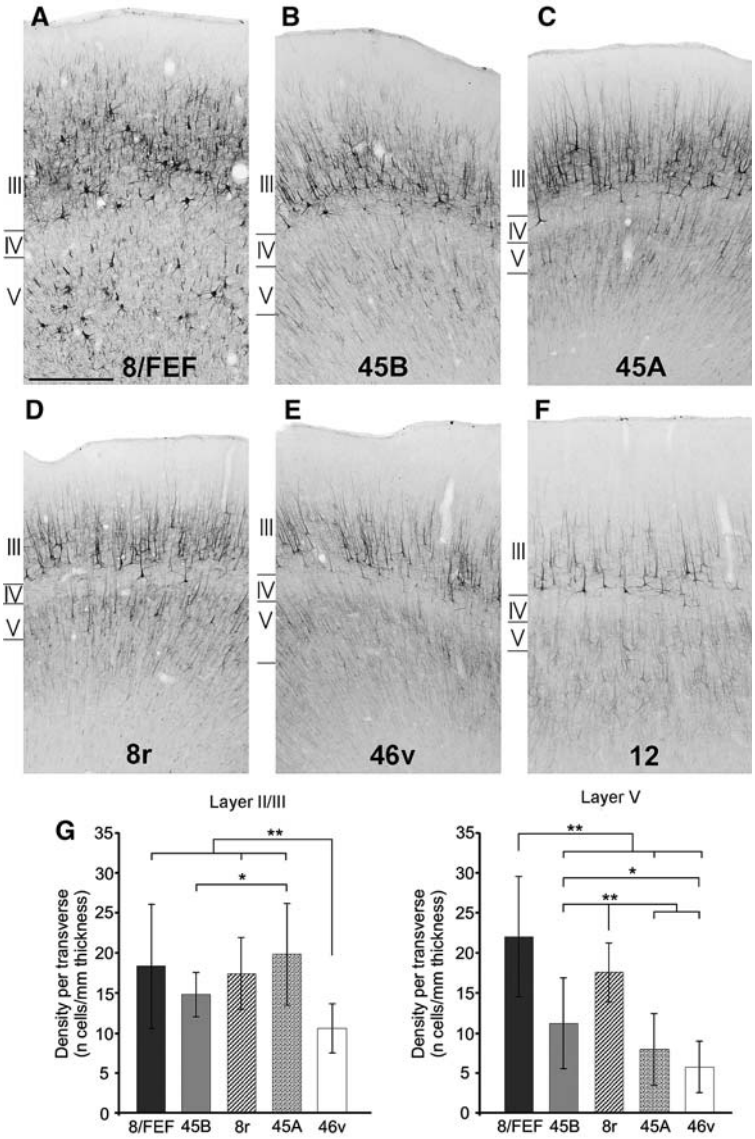

Fig. 14 Distribution of SMI-32ir in the caudal VLPF. Higher magnification views of representative SMI-32 immunostained fields of areas 8/FEF (**a**), 45B (**b**), 45A (**c**), 8r (**d**), 46v (**e**), and 12 (**f**), taken from 18r. The location of all the photomicrographs, but that in **a**, is indicated by *dashed boxes* in Fig. 11b–d. Borders between cortical layers have been reported from adjacent Nissl-stained sections. *Scale bar* = 500 μm in **a** (applies to **a**–**f**). **g** Mean (±SD) values of the density of SMI-32 immunopositive pyramids in layer II/III (*left*) and V (*right*) of areas 8/FEF, 45B, 8r, 45A, and 46v of three Cases (PR17, C18r, and MEF16l). The values are referred to 24 cortical transverses 250 μm wide per area. *Double* and *single asterisks* indicate a significance level of $p < 0.01$ and $p < 0.05$, respectively

language-related Broca's region is not involved in oculomotor functions (see, e.g., Connolly et al. 2007), these connections of area 45 with oculomotor related fields appear at odds with the proposed homology of this area with the corresponding area of the human brain.

The present data, showing that area 45 of Petrides and Pandya (2002) consists of two distinct architectonic entities—45A and 45B—appear helpful for clarifying this apparent discrepancy. Indeed, connectional evidence indicates that both the two frontal oculomotor fields, the FEF and the SEF (Huerta et al. 1987; Huerta and Kaas 1990; Luppino et al. 2003; Stanton et al. 1993; Wang et al. 2005), though with some variability across different studies, appear to be more densely connected with a ventral sector of the prearcuate cortex (area FV of Huerta et al. 1987; area FDi of Stanton et al. 1989), very likely corresponding to area 45B, than with area 45A. The same appears to be true also for the projections from motion sensitive visual areas FST and MST of the caudal superior temporal sulcus (Maioli et al. 1998). Furthermore, a combined 2-deoxyglucose and transneuronal tracing study (Moschovakis et al. 2004) has suggested that the cortical sector activated by the execution of saccadic eye movements and oligosynaptically connected with extraocular motorneurons, extends ventrally to the FEF in the location of area 45B, but not on the convexity cortex, in the location of 45A. Conversely, projections from auditory belt cortex (Romanski et al. 1999b), STG (Petrides and Pandya 1988), and STP (Seltzer and Pandya 1989) appear to target area 45A, but not area 45B. Moreover, Romanski et al. (1999a) observed labeling in auditory cortex following an injection involving areas 12 and 45, but not following an injection in

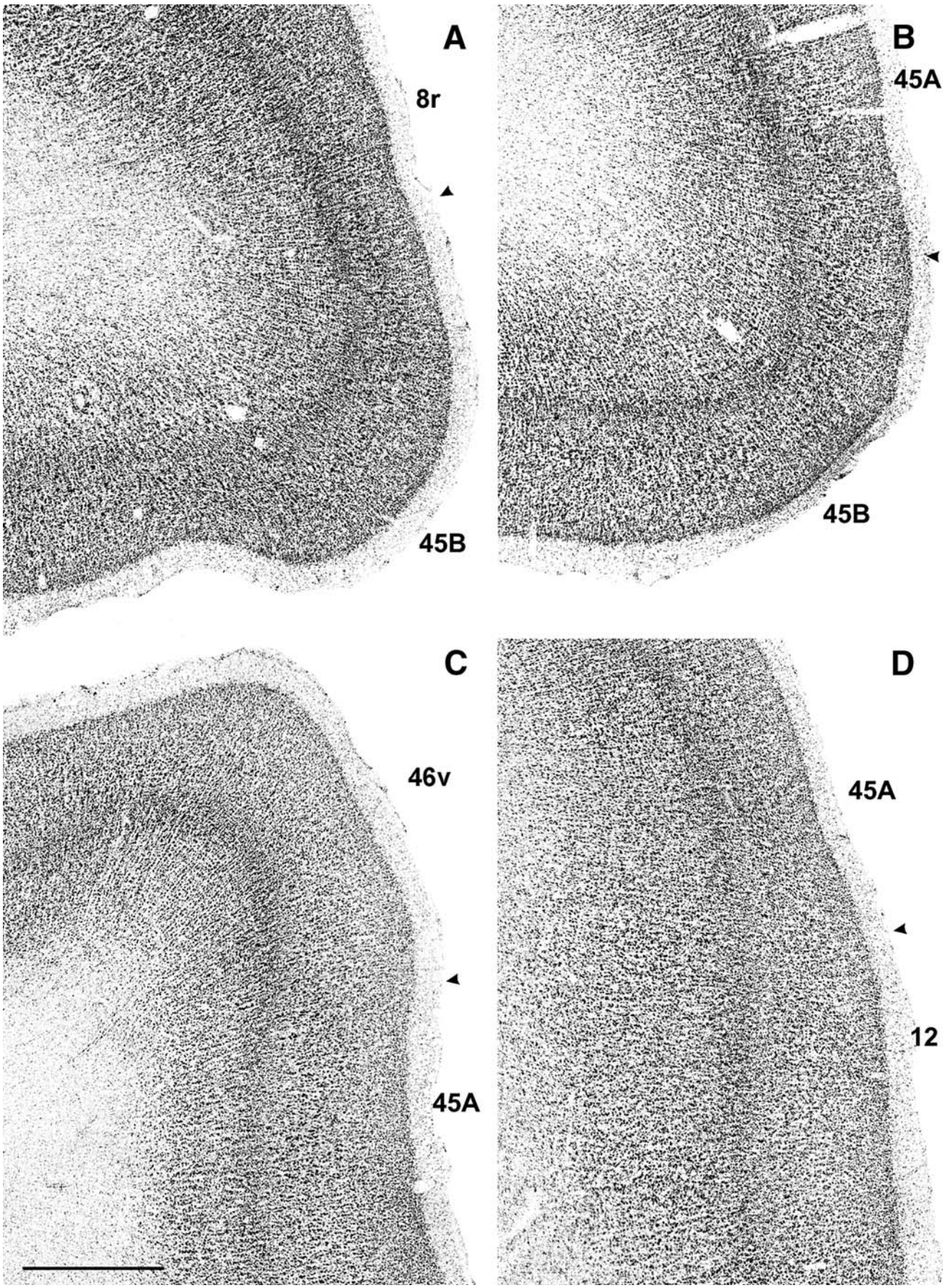
A
8r
45B
B
45A
45B
C
46v
45A
D
45A
12

◀ **Fig. 15** Cytoarchitectonic transitions between caudal VLPF areas. **a** Higher magnification view of the cytoarchitectonic transition between areas 45B and 8r, taken from the section shown in Fig. 3b. **b** Higher magnification view of the cytoarchitectonic transition between areas 45B and 45A, taken from the section shown in Fig. 3c. **c** Higher magnification view of the cytoarchitectonic transition between areas 45A and 46v, taken from the section shown in Fig. 3d. **d** Higher magnification view of the cytoarchitectonic transition between areas 45A and 12 taken from the section shown in Fig. 3d. *Scale bar* = 1 mm in **a** (applies also to **a**–**d**)

the ventral prearcuate bank (likely 45B). Furthermore: (a) auditory and/or visual neurons coding communicative stimuli were recorded just caudal to the IFS, i.e. in area 45A, but not in 45B (Romanski and Goldman-Rakic 2002; Romanski et al. 2005; Sugihara et al. 2006) and (b) face or object selective neurons appear to be located in a sector encompassing both areas 45A and 12, but not 45B (Wilson et al. 1993; O Scalaidhe et al. 1997, 1999). Although, definitive functional and connectional evidence is still needed, all together these data suggest that areas 45B and 45A are not only architectonically, but also functionally and connectionally distinct: area 45B would be a distinct entity of the oculomotor frontal cortex, while area 45A would be a prefrontal area playing a role in the control of communicative behavior. Support in favor of the distinctiveness of area 45A with respect to both areas 45B and 46v has come from recent fMRI data in awake monkeys (Nelissen et al. 2005) showing that observation of shapes and of actions made by others produced three anatomically segregated activation foci in the VLPF, localized in areas 45B, 45A, and 46v.

One further issue raised by the present data relies on the identification of an architectonic area—8r—located in the caudalmost prearcuate convexity. Most connectional studies of this sector have been based on injections limited to the FEF, functionally identified (Huerta et al. 1987; Stanton et al. 1993; Schall et al. 1995; Stanton et al. 1995), or on large injections involving both the prearcuate bank and the adjacent convexity cortex (Barbas and Mesulam 1981; Barbas 1988; Barbas and Pandya 1989). However, Medalla and Barbas (2006) have recently observed that the cortical sector corresponding to area 8r displays a pattern of connectivity with the lateral intraparietal area LIP, different from that of a prearcuate sector corresponding to area 8/FEF. These data suggest that the prearcuate bank and the prearcuate convexity (likely 8/FEF and 8r, respectively) differ not only in terms of overall neuronal density, but also, at least in part, in their cortical connections.

In the functional literature, this cortical sector has been often included into a larger caudal prefrontal region, extending also into caudal area 46, considered to be involved in visuospatial functions and in spatial working memory (see, e.g., Levy and Goldman-Rakic 2000; Romanski 2004). Recent data, however, have shown that the caudal prearcuate convexity: (a) similarly to area 45B, is activated by the execution of saccadic eye movements and is a source of oligosynaptic projections to the extraocular muscles (Moschovakis et al. 2004); (b) appears to be selectively involved in vergence and ocular accommodation, and in the sensorimotor transformations required for these eye movements (Gamlin and Yoon 2000); (c) contains a class of direction selective visually responsive neurons which appear to play an important executive role during the execution of a direction discrimination task in which the sample and test stimuli were separated by a brief

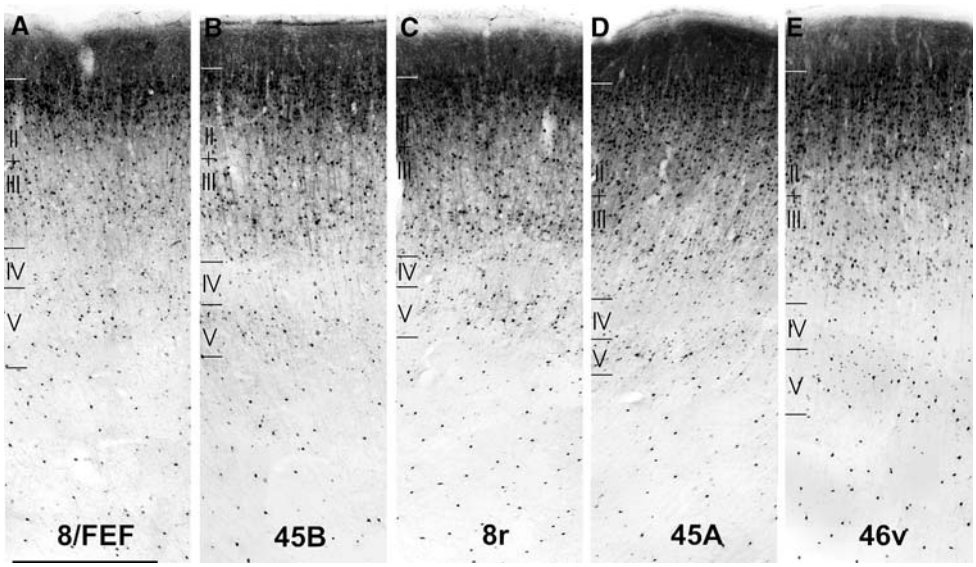

Fig. 16 Distribution of CBir in the caudal VLPF. Higher magnification views of representative CB immunostained fields of areas 8/FEF (**a**), 45B (**b**), 8r (**c**), 45A (**d**), and 46v (**e**), taken from Case PR17. *Scale bar* = 500 μm in **a** (applies to **a**–**e**)

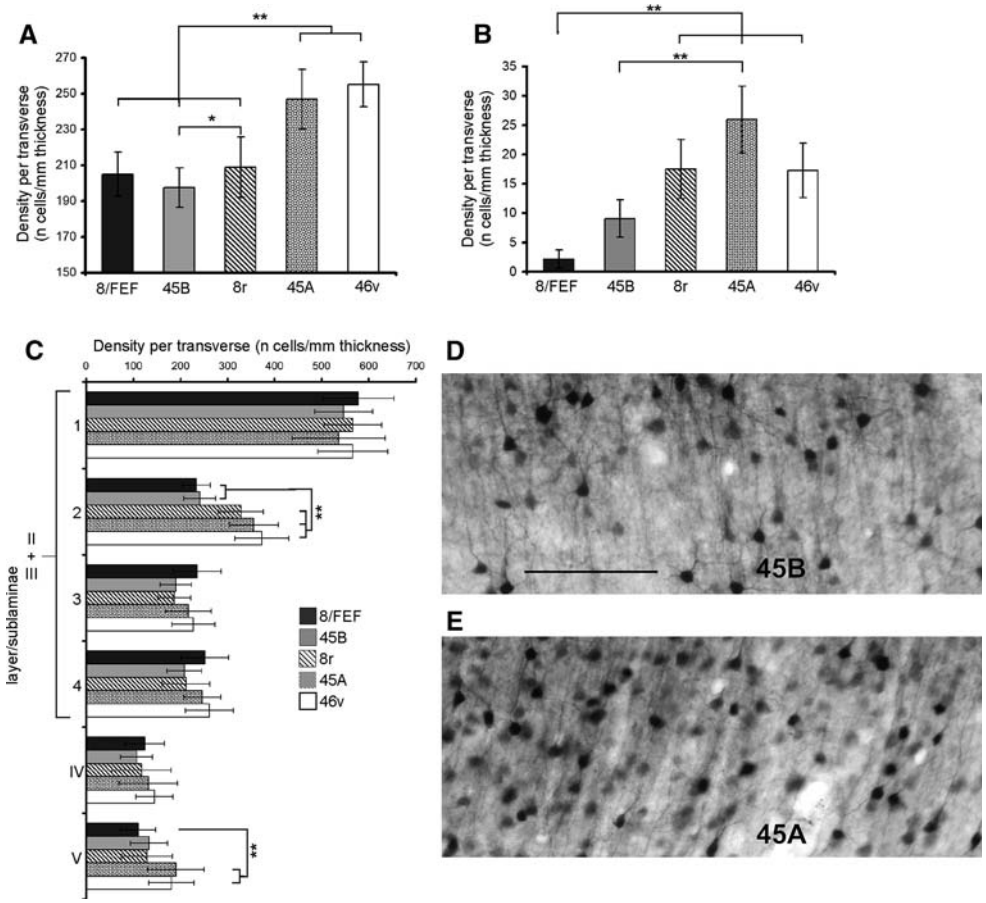

Fig. 17 Distribution of CBir in the caudal VLPF. Mean (±SD) values of the density of CB immunopositive layers I–V nonpyramidal (**a**) and pyramidal (**b**) neurons and laminar density of CB immunopositive nonpyramidal neurons (**c**) of areas 8/FEF, 45B, 8r, 45A, and 46v of three Cases (PR17, M3l, and MEF16l). The values are referred to 24 cortical transverses of 250 μm width per area. For the analysis of the laminar density, layers II plus III have been subdivided into four sublaminae of equal thickness. *Double* and *single asterisks* indicate a significance level of $p < 0.01$ and $p < 0.05$, respectively. Higher power photomicrographs centred on the second layer II/III sublamina of areas 45B (**d**) and 45A (**e**). *Scale bar* = 100 μm in **d**, applies also to **e**

Table 2 Salient architectonic features of the caudal VLPF areas

Area	Nissl	Myelin	SMI-32ir
8/FEF	Many medium sized layer III pyramids Many large layer V pyramids[a]	Highly myelinated. Dense and wide horizontal fiber plexus[a]	Layer III rich in positive apical dendrites and cell bodies Large, layer V positive cells[a] High layer V positive cell density[c]
45B	Large, deeply stained layer III pyramids[a] Relatively cell sparse layer V with rare large pyramids[b]	Highly myelinated Dark outer band of Baillarger[b]	Layer III rich in positive apical dendrites and cell bodies Large, layer III positive cells[b] Small layer V positive cell Low layer V positive cell density[c]
8r	Thin, homogeneous layer III[b] Prominent layer V with densely packed small pyramids[a]	Moderately myelinated[b] Outer band of Baillarger; lighter than the inner one[b]	Relatively small amount of positive apical dendrites and sparser positive cells in layer III[b] Small layer V positive cells High layer V positive cell density[c]
45A	Dense medium sized pyramids in lower layer III[a] Relatively dense layer V	Highly myelinated[b] Dark outer and inner bands of Baillager[b]	Layer III rich in positive apical dendrites and medium sized pyramids Cell density in layer III higher than in area 45B[c] Low layer V positive cell density[c]
46v	Dense, homogeneous layer III[b] Cell dense layers IV and V	Lightly myelinated[b] Both bands of Baillarger evident[b]	Lower content of positive dendrites in layer III and of positive cells in layers III and V[a] Low layers III and V positive cell density[c]

Table 2 continued

Area	Nissl	Myelin	SMI-32ir
12	Cell dense layer III with slight increase in cell size in the lower part[b] Sublaminated layer V[b]	Moderately myelinated[b] Both bands of Baillarger evident	Sparse, darkly stained cells in lower layer III[b] Very low content of positive apical dendrites in layer III[b]

[a] Identifying architectonic feature

[b] Distinguishes area from some of its neighbor

[c] Based on quantitative analysis

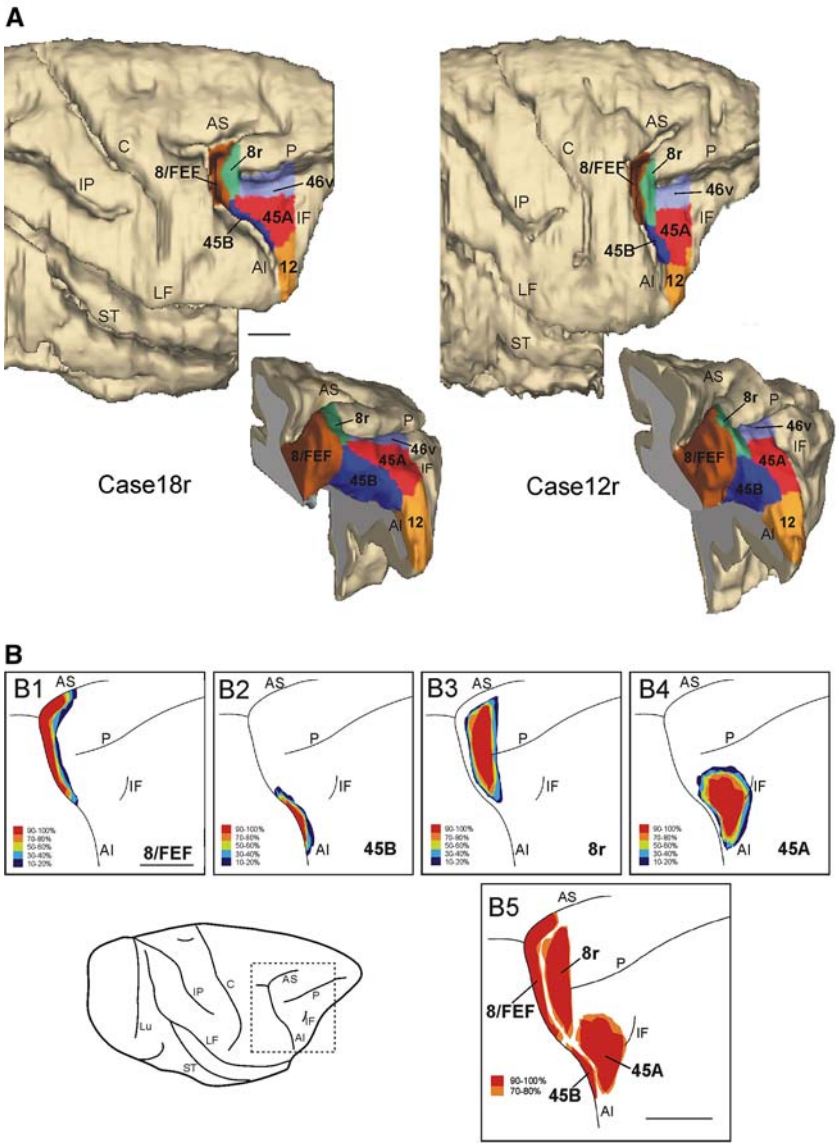

Fig. 18 Location and extent of caudal VLPF areas. **a** 3D reconstructions of the frontal lobe of Cases 18r and 12r. For each case, the frontal lobe is shown from a dorso-lateral view (*scale bar* = 5 mm, for both reconstructions) and from a caudolateral view in which the anterior bank of the IAS was exposed with dissection of the 3D reconstruction along its fundus. **b** Average location of 8/FEF (*B1*), 45B (*B2*), 8r (*B3*), and 45A (*B4*) obtained by warping 2D reconstructions of ten cytoarchitectonic maps from seven *Macaca nemestrina* and two *M. fascicularis* to fit with a template frontal lobe. The degree of overlap of the individual maps is shown with a color scale from *red* (overlap of at least nine maps) to *blue* (overlap of no more than two maps). *Scale bar* = 5 mm in *B1* (applies to *B1–B4*). *B5* shows an overall view of the convexity cortex occupied by areas 8/FEF, 45B, 8r, and 45A in at least nine (*red*) or seven (*orange*, the areal *core*) maps. *Scale bar* = 5 mm. *Dashed box* on the brain drawing indicates the area shown enlarged in *B1–B5*. Abbreviations as in Figs. 1, 2, and 3

memory delay (Zaksas and Pasternak 2006). These data suggest that area 8r represents a further independent field of the frontal oculomotor cortex, distinct from the FEF and the caudal part of area 46.

Acknowledgments This study was supported by MIUR (PRIN 2006, no. 2006052343_002). A.B. is supported by a fellowship from EU (Marie Curie, Early stage training program "Sensoprim" MEST-CT-2004-007825). The 3D reconstruction software was developed by

CRS4, Pula, Cagliari, Italy. We thank L. Riggio and L. Bonini for valuable help in the statistical analysis and W. Depuydt for developing warping software.

References

Barbas H (1988) Anatomic organization of basoventral and mediodorsal visual recipient prefrontal regions in the rhesus monkey. J Comp Neurol 276:313–342

Barbas H, Mesulam M-M (1981) Organization of afferent input to subdivision of area 8 in the rhesus monkey. J Comp Neurol 200:407–431

Barbas H, Mesulam MM (1985) Cortical afferent input to the principalis region of the rhesus monkey. Neuroscience 15:619–637

Barbas H, Pandya DN (1989) Architecture and intrinsic connections of the prefrontal cortex in the rhesus monkey. J Comp Neurol 286:353–375

Bettio F, Demelio S, Gobbetti E, Luppino G, Matelli M (2001) Interactive 3-D reconstruction and visualization of primates cerebral cortex. Soc Neurosci Abstr Program No. 728.724

von Bonin G, Bailey P (1947) The neocortex of *Macaca mulatta*. University of Illinois Press, Urbana

Brodmann K (1905) Beitraege zur histologischen Lokalisation der Grosshirnrinde. III. Mitteilung. Die Rindenfelder der niederen Affen. J Psychol Neurol 4:177–266

Bruce CJ, Goldberg ME (1984) Physiology of the frontal eye fields. Trends Neurosci 7:436–441

Bruce CJ, Goldberg ME, Bushnell C, Stanton GB (1985) Primate frontal eye fields. II. Physiological and anatomical correlates of electrically evoked movements. J Neurophysiol 54:714–734

Cadoret G, Bouchard M, Petrides M (2000) Orofacial representation in the rostral bank of the inferior ramus of the arcuate sulcus of the monkey. Soc Neurosci Abstr Program No. 253.13

Calzavara R, Zappala A, Rozzi S, Matelli M, Luppino G (2005) Neurochemical characterization of the cerebellar-recipient motor thalamic territory in the macaque monkey. Eur J Neurosci 21:1869–1894

Campbell MJ, Morrison JH (1989) Monoclonal antibody to neurofilament protein (SMI-32) labels a subpopulation of pyramidal neurons in the human and monkey neocortex. J Comp Neurol 282:191–205

Carmichael ST, Price JL (1994) Architectonic subdivision of the orbital and medial prefrontal cortex in the macaque monkey. J Comp Neurol 346:366–402

Carmichael ST, Price JL (1995a) Limbic connections of the orbital and medial prefrontal cortex in macaque monkeys. J Comp Neurol 363:615–641

Carmichael ST, Price JL (1995b) Sensory and premotor connections of the orbital and medial prefrontal cortex of macaque monkeys. J Comp Neurol 363:642–664

Condé F, Lund JS, Jacobowitz DM, Baimbridge KG, Lewis DA (1994) Local circuit neurons immunoreactive for calretinin, calbindin D-28k or parvalbumin in monkey prefrontal cortex: distribution and morphology. J Comp Neurol 341:95–116

Connolly JD, Goodale MA, Cant JS, Munoz DP (2007) Effector-specific fields for motor preparation in the human frontal cortex. NeuroImage 34:1209

Cusick CG, Seltzer B, Cola M, Griggs E (1995) Chemoarchitectonics and corticocortical terminations within the superior temporal sulcus of the rhesus monkey: evidence for subdivisions of superior temporal polysensory cortex. J Comp Neurol 360:513–535

DeFelipe J, Hendry SH, Jones EG (1989) High-resolution light and electron microscopic immunohistochemistry of colocalized GABA and calbindin D-28k in somata of double bouquet cell axons of monkey somatosensory cortex. Eur J Neurosci 4:46–60

Dombrowski SM, Hilgetag CC, Barbas H (2001) Quantitative architecture distinguishes prefrontal cortical systems in the rhesus monkey. Cereb Cortex 11:975–988

Galletti C, Gamberini M, Kutz DF, Fattori P, Luppino G, Matelli M (2001) The cortical connections of area V6: an occipito-parietal network processing visual information. Eur J Neurosci 13:1572–1588

Gallyas F (1979) Silver staining of myelin by means of physical development. Neurol Res 1:203–209

Gamlin PD, Yoon K (2000) An area for vergence eye movement in primate frontal cortex. Nature 407:1003

Geyer S, Zilles K, Luppino G, Matelli M (2000) Neurofilament protein distribution in the macaque monkey dorsolateral premotor cortex. Eur J Neurosci 12:1554–1566

Gregoriou GG, Borra E, Matelli M, Luppino G (2006) Architectonic organization of the inferior parietal convexity of the macaque monkey. J Comp Neurol 496:422–451

Hendry SH, Jones EG, Emson PC, Lawson DE, Heizmann CW, Streit P (1989) Two classes of cortical GABA neurons defined by differential calcium binding protein immunoreactivities. Exp Brain Res 76:467–472

Hof PR, Morrison JH (1995) Neurofilament protein defines regional patterns of cortical organization in the macaque monkey visual system: a quantitative immunohistochemical analysis. J Comp Neurol 352:161–186

Hof PR, Glezer II, Conde F, Flagg RA, Rubin MB, Nimchinsky EA, Vogt Weisenhorn DM (1999) Cellular distribution of the calcium-binding proteins parvalbumin, calbindin, and calretinin in the neocortex of mammals: phylogenetic and developmental patterns. J Chem Neuroanat 16:77

Huerta MF, Kaas JH (1990) Supplementary eye field as defined by intracortical microstimulation: connections in Macaques. J Comp Neurol 293:299–330

Huerta MF, Krubitzer LA, Kaas JH (1987) Frontal eye field as defined by intracortical microstimulation in squirrel monkeys, owl monkeys, and macaque monkeys II. Cortical connections. J Comp Neurol 265:332–361

Kondo H, Tanaka K, Hashikawa T, Jones EG (1994) Neurochemical gradients along the monkey occipito-temporal cortical pathway. Neuroreport 5:613–616

Kondo H, Tanaka K, Hashikawa T, Jones EG (1999) Neurochemical gradients along monkey sensory cortical pathways: calbindin-immunoreactive pyramidal neurons in layers II and III. Eur J Neurosci 11:4197–4203

Levy R, Goldman-Rakic PS (2000) Segregation of working memory functions within the dorsolateral prefrontal cortex. Exp Brain Res 133:23–32

Luppino G, Calzavara R, Rozzi S, Matelli M (2001) Projections from the superior temporal sulcus to the agranular frontal cortex in the macaque. Eur J Neurosci 14:1035–1040

Luppino G, Belmalih A, Borra E, Gerbella M, Rozzi S (2006) Architectonics and cortical connections of the ventral prearcuate area 45B of the macaque monkey. Soc Neurosci Abstr Program No. 63.2

Luppino G, Rozzi S, Calzavara R, Matelli M (2003) Prefrontal and agranular cingulate projections to the dorsal premotor areas F2 and F7 in the macaque monkey. Eur J Neurosci 17:559–578

Maioli MG, Squatrito S, SamolskyDekel BG, Sanseverino ER (1998) Corticocortical connections between frontal periarcuate regions and visual areas of the superior temporal sulcus and the adjoining inferior parietal lobule in the macaque monkey. Brain Res 789:118–125

Medalla M, Barbas H (2006) Diversity of laminar connections linking periarcuate and lateral intraparietal areas depends on cortical structure. Eur J Neurosci 23:161–179

Moschovakis AK, Gregoriou GG, Ugolini G, Doldan M, Graf W, Guldin W, Hadjidimitrakis K, Savaki HE (2004) Oculomotor areas of the primate frontal lobes: a transneuronal transfer of rabies virus and [14C]-2-deoxyglucose functional imaging study. J Neurosci 24:5726–5740

Nelissen K, Luppino G, Vanduffel W, Rizzolatti G, Orban GA (2005) Observing others: multiple action representation in the frontal lobe. Science 310:332–336

Nimchinsky EA, Hof PR, Young WG, Morrison JH (1996) Neurochemical, morphologic, and laminar characterization of cortical projection neurons in the cingulate motor areas of the macaque monkey. J Comp Neurol 374:136–160

O Scalaidhe SP, Wilson FAW, Goldman-Rakic PS (1997) Areal segregation of face-processing neurons in prefrontal cortex. Science 278:1135–1138

O Scalaidhe SP, Wilson FAW, Goldman-Rakic PS (1999) Face-selective neurons during passive viewing and working memory performance of rhesus monkeys: evidence for intrinsic specialization of neuronal coding. Cereb Cortex 9:459–475

Passingham RE (1993) The frontal lobe and voluntary action. Oxford University Press, Oxford

Passingham RE, Toni I, Rushworth MFS (2000) Specialisation within the prefrontal cortex: the ventral prefrontal cortex and associative learning. Exp Brain Res 133:103–113

Petrides M (2005) Lateral prefrontal cortex: architectonic and functional organization. Philos Trans R Soc B Biol Sci 360:781

Petrides M, Pandya DN (1988) Association fiber pathways to the frontal cortex from the superior temporal region in the rhesus monkey. J Comp Neurol 273:52–66

Petrides M, Pandya DN (1994) Comparative architectonic analysis of the human and the macaque frontal cortex. In: Boller F, Grafman J (eds) Handbook of neuropsychology. Elsevier, Amsterdam, pp 17–58

Petrides M, Pandya DN (1999) Dorsolateral prefrontal cortex: comparative cytoarchitectonic analysis in the human and the macaque brain and corticocortical connection patterns. Eur J Neurosci 11:1011–1036

Petrides M, Pandya DN (2002) Comparative cytoarchitectonic analysis of the human and the macaque ventrolateral prefrontal cortex and corticocortical connection patterns in the monkey. Eur J Neurosci 16:291–310

Preuss TM, Goldman-Rakic PS (1989) Connections of the ventral granular frontal cortex of macaques with perisylvian premotor and somatosensory areas: anatomical evidence for somatic representation in primate frontal association cortex. J Comp Neurol 282:293–316

Preuss TM, Goldman-Rakic PS (1991) Myelo- and cytoarchitecture of the granular frontal cortex and surrounding regions in the streptisine primate *Galago* and the anthropoid primate *Macaca*. J Comp Neurol 310:429–474

Romanski LM (2004) Domain specificity in the primate prefrontal cortex. Cogn Affect Behav Neurosci 4:421–429

Romanski LM, Goldman-Rakic PS (2002) An auditory domain in primate prefrontal cortex. Nat Neurosci 5:15

Romanski LM, Bates JF, Goldman-Rakic PS (1999a) Auditory belt and parabelt projections to the prefrontal cortex in the rhesus monkey. J Comp Neurol 403:141–157

Romanski LM, Tian B, Fritz J, Mishkin M, Goldman-Rakic PS, Rauschecker JP (1999b) Dual streams of auditory afferents target multiple domains in the primate prefrontal cortex. Nat neurosci 2:1131–1136

Romanski LM, Averbeck BB, Diltz M (2005) Neural representation of vocalizations in the primate ventrolateral prefrontal cortex. J Neurophysiol 93:734–747

Rozzi S, Calzavara R, Belmalih A, Borra E, Gregoriou GG, Matelli M, Luppino G (2006) Cortical connections of the inferior parietal cortical convexity of the macaque monkey. Cereb Cortex 16:1389–1417

Schall JD, Morel A, King DJ, Bullier J (1995) Topography of visual cortex connections with frontal eye field in macaque: convergence and segregation of processing streams. J Neurosci 15:4464–4487

Seltzer B, Pandya DN (1989) Frontal lobe connections of the superior temporal sulcus in the rhesus monkey. J Comp Neurol 281:97–113

Stanton GB, Deng S-Y, Goldberg ME, McMullen NT (1989) Cytoarchitectural characteristics of the frontal eye fields in macaque monkeys. J Comp Neurol 282:415–427

Stanton GB, Bruce CJ, Goldberg ME (1993) Topography of projections to the frontal lobe from the macaque frontal eye fields. J Comp Neurol 330:286–301

Stanton GB, Bruce CJ, Goldberg ME (1995) Topography of projections to posterior cortical areas from the macaque frontal eye fields. J Comp Neurol 353:291–305

Sugihara T, Diltz MD, Averbeck BB, Romanski LM (2006) Integration of auditory and visual communication information in the primate ventrolateral prefrontal cortex. J Neurosci 26:11138–11147

Walker E (1940) A cytoarchitectural study of the prefrontal area of the macaque monkey. J Comp Neurol 98:59–86

Wang Y, Isoda M, Matsuzaka Y, Shima K, Tanji J (2005) Prefrontal cortical cells projecting to the supplementary eye field and presupplementary motor area in the monkey. Neurosci Res 53:1

Watson DE (1992) Contouring: a guide to the analysis and display of spatial data. Pergamon (Elsevier), Tarrytown

Wilson FA, Scalaidhe SP, Goldman-Rakic PS (1993) Dissociation of object and spatial processing domains in primate prefrontal cortex. Science 260:1955–1958

Zaksas D, Pasternak T (2006) Directional signals in the prefrontal cortex and in area MT during a working memory for visual motion task. J Neurosci 26:11726–11742